Semiconductor Quantum-Well Structures for Optoelectronics–Recent Advances and Future Prospects–

JAPANESE JOURNAL OF APPLIED PHYSICS
VOL. 26, NO. 3, MARCH, 1987, pp. 315-330

—Invited paper—

Semiconductor Quantum-Well Structures for Optoelectronics —Recent Advances and Future Prospects—

Hiroshi OKAMOTO

NTT Electrical Communications Laboratories, 3-9-11, Midori-cho, Musashino-shi, Tokyo 180

(Received September 5, 1986; accepted for publication December 20, 1986)

Due to the quantum size effect, semiconductor quantum-well structure exhibits many unique material properties which can not be realized in conventional bulk crystals. These unique properties are very attractive for novel electronic and optoelectronic devices. This paper reviews studies on physical properties and application of quantum well structures for optoelectronics, and gives a future forecasting in the progress of this field.

§1. Introduction

A quantum-well (QW) structure is a finite segment of a superlattice which is a one-dimensional periodic structure consisting of alternating ultra-thin layers of two different materials. Research on semiconductor superlattices was initiated by the proposal of a negative resistance due to electron transport through multiple wells and barriers made by Esaki and Tsu.[1] If characteristic diemsnions such as the superlattice period, layer thicknesses (the QW layer thickness, L_z, and the barrier layer thickness, L_B), etc., in semiconductor nanometer structures are reduced to less than the electron mean free path, the entire electron system enters into a quantum regime (*quantum size effect*).

Due to the quantization of the wavefunction in one direction (z-direction, which is the growth direction of the epitaxial layer) in the QW layer confined by the barrier layers as shown in Fig. 1, the energy dependence of the density-of-states $\rho(E)$ for electrons and/or holes changes to a staircase form. (In this paper, a QW layer means a potential well layer, while a QW structure means a structure including QW layers and barrier layers and it sometimes includes a superlattice.) This is the first important point, which was emphasized first by Dingle in 1975.[2] In a bulk crystal where the minimum of the characteristic sizes is beyond the carrier mean free path, $\rho(E)$ is always parabolic and it is equal to zero at the

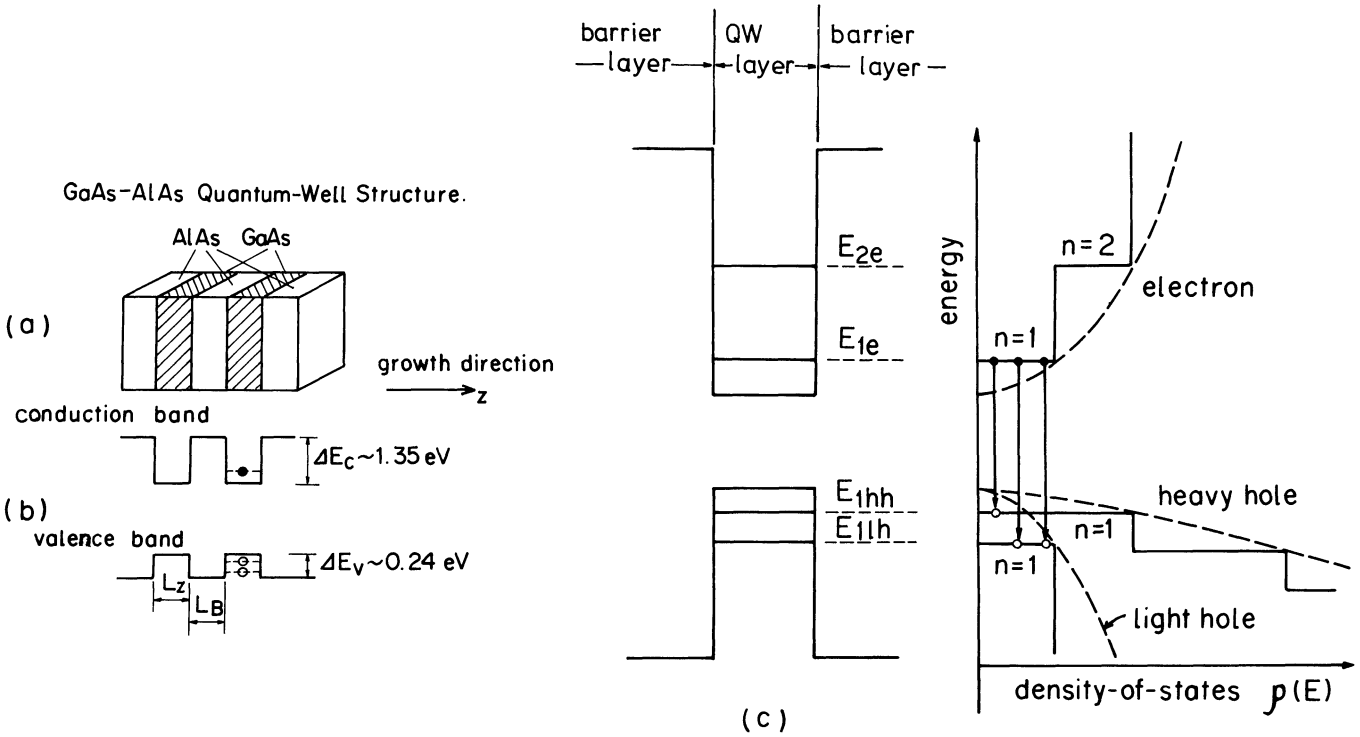

Fig. 1. GaAs-AlAs quantum-well structure. (a) Layer structure. z-direction is the growth direction. (b) Energy band structure for conduction and valence band. (c) Quantum energy levels in a quantum well. E_{1e} and E_{2e} are $n=1$ and $n=2$ electron levels, and E_{1hh} and E_{11h} are $n=1$ heavy-hole and light-hole levels, respectively. (d) Density-of-states as a function of energy for a QW structure (solid line) and for a bulk crystal (broken line).

minimum energy (i.e., at the band edge). Different crystals with different constituent elements do not change this situation but only give different values of the curvature of the parabolic $\rho(E)$ curve. In contrast to the bulk crystal, the staircase form of $\rho(E)$ in the QW structure has a finite non-zero value of density-of-states even at the minimum energy. Furthermore, the detailed form of the staircase curve can be tailored by controlling the structure parameters such as L_z and/or L_B. In other words, the artificial arrangement of constituent atoms brings about a perfectly new form of $\rho(E)$ for the material made even from the most familiar atoms such as Al, Ga, and As. This new concept, *the density-of-states modification*, was attractive enough to accelerate the advancement of crystal growth technology, including molecular beam epitaxy (MBE) and metal-organic chemical vapor deposition (MO-CVD), by which QW structures are grown, and it was dvantageously used also in novel devices, such as QW laser diodes. Tsang[3] demonstrated in 1981 that multi-quantum-well (MQW) laser diodes grown by improved MBE exhibited a very low threshold current density. This achievement triggered studies of understanding the device physics in this new type of laser diodes. As a result, many significant characteristics, which are not present in converntional (bulk-type) laser diodes, have been found which will be described in §4.

The two-dimensional exciton is an another feature of the QW structure. Due to the confinement of excitons in a layer whose thickness is smaller than the excitonic Bohr diameter (28 nm in GaAs), the binding energy and oscillator strength of the exciton increase, and consequently, excitonic states become stable even at room-temperature (*room-temperature exciton*). The first observation of the exciton peaks in an optical absorption spectrum of a superlattice at room-temperature in 1981 by Ishibashi *et al.*[4] has stimulated the studies on exciton-associated-physics, including the optical non-linearity and the electric field effect, and as a result, many novel optical functional devices have been proposed, which will be discussed in §5.

The concept of modulation doping was proposed by Dingle *et al.* in 1978.[5] Spatial separation of electrons (or holes) from their host donors (or acceptors) yielded the two-dimensional electron (or hole) gas whose mobility are extraordinarily higher than ever realized in conventional semiconductors. A new high-speed electronic device was conceived, which is now called high electron mobility transistor (HEMT),[6] Although the two-dimensional carrier gas will also be attractive for optoelectronics, at the present stage the interest is limited, so that it is beyond the scope of this paper.

Compositional disordering of superlattices or QW structures by diffusion or ion implantation of impurity atoms, which was first demonstrated by Laidig *et al.*,[7] has a two-fold significance. It is important to get deeper insight into the apparently well-known phenomenon of impurity diffusion. In addition, the compositional disordering can be considered as an attractive method for *material modification*. This is because the compositionally disordered material exhibits properties, such as bandgap energy, optical refractive index, etc., different from those of the original superlattice or QW structure. This material modification has been utilized not only to simplify the fabrication process of advanced MQW laser diodes, but also to fabricate a quantum-well-wire structure in which carriers are confined both in the thickness direction and also in lateral direction. The resulting two-dimensional quantum size effect will be studied in near future. These topics will be described in §6.

The advancement in the research and application of QW structures is strongly correlated to the progress in the related material technologies, such as epitaxial growth (MBE, MO-CVD, etc.), characterization (Auger electron spectroscopy (AES), secondary ion mass spectroscopy (SIMS), transmission electron microscopy (TEM), and other micro-characterization technologies) and processing (focused ion beam (FIB) technology, electron beam lithography, and so on). The progress in these fields is very important. But, details are not fully described in this paper, so that the reader is referred to the relevant text books.[8]

In the following, the description is mostly limited to GaAs-$Al_xGa_{1-x}As$ QW structures grown on (100) GaAs substrates by MBE. Crystal perfection of QW or superlattice epitaxial layers is discussed first in §2. Optical properties specific to the QW structures are described in §3. In §4, QW laser diodes are compared with conventional bulk-type double-heterostructure (DH) lasers. GaSb-$Al_xGa_{1-x}Sb$ QW lasers which emit in the long wavelength region are also described briefly. Room-temperature exciton related new optical devices are presented in §5. Material modification and quantum-well wire and box structures are discussed in Section 6 as an example of the future scope.

§2. Structural Perfection

One of the simplest diagnostics of the epitaxial layer is a visual inspection of its surface morphology. At the beginning of of 1980s, when the MBE growth technology was still immature, the surface of mixed alloy $Al_xGa_{1-x}As$ films grown by MBE often appeared hazy especially when the growth temperature was below 600°C. In a marked contrast, the surface of a GaAs-AlAs superlattice epilayer grown under identical conditions always looked featureless.[4] In relation to this observation, Gossard *et al.*[9] reported an enhancement of the photoluminescence (PL) efficiency from a QW layer by a factor of 10 or more when a superlattice buffer layer was introduced between the substrate and the epitaxial QW layer. These phenomena were interpreted by Chai *et al.*[10] in terms of accommodation of misfit strain in the superlattice layers, which is the basic principle of strained-layer superlattices, and later by Petroff *et al.*[11] in terms of impurity gettering effects during the growth of superlattices. But these interpretations are still controversial. Recent measurements by Iwamura *et al.** demonstrated that the PL efficiency enhancement is preserved from the weak excitation range (below 1 W/cm^2) up to strong excitation with more than 100 kW/cm^2,

*H. Iwamura *et al.* private communication.

which rules out any possibility of deep level related mechanism for the enhancement. Furthermore, in spite of the PL enhancement, the threshold power density for photo-pumped laser operation does not differe at all for QW wafers with and without superlattice buffer layer.

The quantized energy in a QW layer shown in Fig. 1 is in inverse proportion to the square of its layer thickness L_z. In order to extract optical properties intrinsic to the QW layer, especially to the multiple QW layers, L_z must be uniform over the whole QW layers. In addition, the QW structure must have good smoothness and abruptness at the hetero-interface between a QW layer and a barrier layer because these factors have a significant influence on the optical properties, especially the exciton behavior. These requirements accelerated refinements both in the material growth technology and in the material characterization technology up to a level of an atomic scale.

In the MBE technology, Harris, Neave *et al.*[12,13] reported in 1983 that the reflection high energy electron diffraction (RHEED) signal from a growing wafer changes its intensity in an oscillatory manner. The period of the oscillation is exactly equal to the growth of one monolayer. The phenomenon can be used not only for *in-situ* measurements of the accurate growth rate but also for the accurate timing to open and close the effusion cell shutters necessary to grow QW structure epitaxial layers. Although this technology is very convenient, it does not guarantee the growth with atomically flat hetero-interface. Furthermore, the RHEED intensity oscillation becomes difficult to observe when the growth is performed at a substrate temperature exceeding 600°C, which is necessary for GaAs-$Al_xGa_{1-x}As$ epilayer growth with excellent optical quality.

To measure L_z and L_B of grown MQW wafers, the X-ray diffraction method[14] is conveniently used because it is a non-destructive method. In the X-ray diffraction pattern, many diffraction peaks appear, one being from the substrate and the others being the fundamental and the higher order diffractions from the MQW layer. The higher order diffractions originate from the existence of the longer period (L_z+L_B) in the structure, while the fundamental one reflects the average Al content of the MQW structure, which is equal to $L_B/(L_z+L_B)$ in the case of a GaAs-AlAs MQW. The X-ray method is suited for MQW samples whose total thickness is larger than the extinction length of the X-ray.

To obtain insight into the smoothness of the hetero-interface between a QW layer and a barrier layer, PL measurements are a non-destructive and now widely used method. The real QW layer is not uniform in L_z within the layer but it is an assembly of lateral islands within each of which L_z is perfectly uniform so as to give a definite value of the quantized energy level and therefore give a definite value of the PL energy which is given by the transition energy from the $n=1$ electron level $E_{1e}(L_z)$ to the $n=1$ heavy-hole level $E_{1hh}(L_z)$ minus the exciton binding energy $E_{ex}(L_z)$, that is,

$$h\nu_{PL}=E_g+E_{1e}(L_z)+E_{1hh}(L_z)-E_{ex}(L_z) \quad (1)$$

where E_g is the bandgap energy of GaAs. The adjacent lateral island has another thickness L_z' which is different from L_z by an integral multiple of the monolayer thickness $a_0/2=2.83$ Å and therefore gives a PL energy $h\nu'_{PL}$ which differs from $h\nu_{PL}$. When the lateral extent W of the island is larger than the Bohr diameter $(2a_B)$ of the exciton, the PL spectrum has a multiple peak structure with different energies from different islands. In the other case with $W \ll 2a_B$, an exciton experiences different values of L_z, thereby giving rise to a spectral broadening of the PL. In the latter case the broadening ΔE can be roughly estimated to be

$$\Delta E=(\hbar^2/m_e^*)(\Delta L_z/L_z^3) \quad (2)$$

where m_e^* is the effective electron mass and ΔL_z is the average inhomogeneity in L_z. Figure 2 shows the full width at half maximum (FWHM) of the PL spectra as a function of L_z for GaAs-AlAs and GaAs-$Al_{0.3}Ga_{0.7}As$ MQW structures, which was first measured by Goldstein *et al.*[15] The broadening is larger for MQWs with higher potential barriers. In both types of MQWs, the FWHM increases when L_z becomes small. From this result we can estimate that the average irregularity ΔL_z is not more than the one monolayer thickness $a_0/2$. Recently it was reported that interruption of MBE grown at the hetero-interface brings a drastic reduction of PL FWHM. This phenomenon is interpreted in a way that the lateral size of the island grows during the interruption period[16-17] due to the surface migration of group III atoms.

In order to confirm the smoothness and abruptness of the hetero-interface, the cross section of the grown wafer is examined by TEM. Pioneering studies were done by Petroff.[18] A dark field image using a satellite diffraction spot pertinent to the superlattice revealed the layer structure with a resolution of two monolayers. The lattice arrangement and defects were first observed by the author's group[19] by observing a lattice image which was reconstructed through the interference between the direct (000) beam and several of the low index diffraction beams. However, under the high magnification for the lattice image observation, it was difficult to obtain contrast

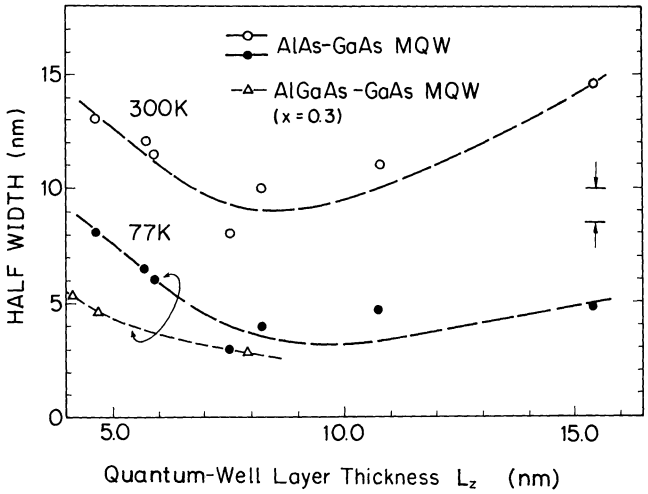

Fig. 2. Full width at half maximum of photoluminescence spectrum for GaAs-AlAs and GaAs-$Al_{0.3}Ga_{0.7}As$ MQW structure as a function of the potential well layer thickness L_z. Closed and solid circles are for GaAs-AlAs MQW measured at 300 and 77 K, respectively. Triangles are for GaAs-$Al_{0.3}Ga_{0.7}As$ MQW measured at 77 K.

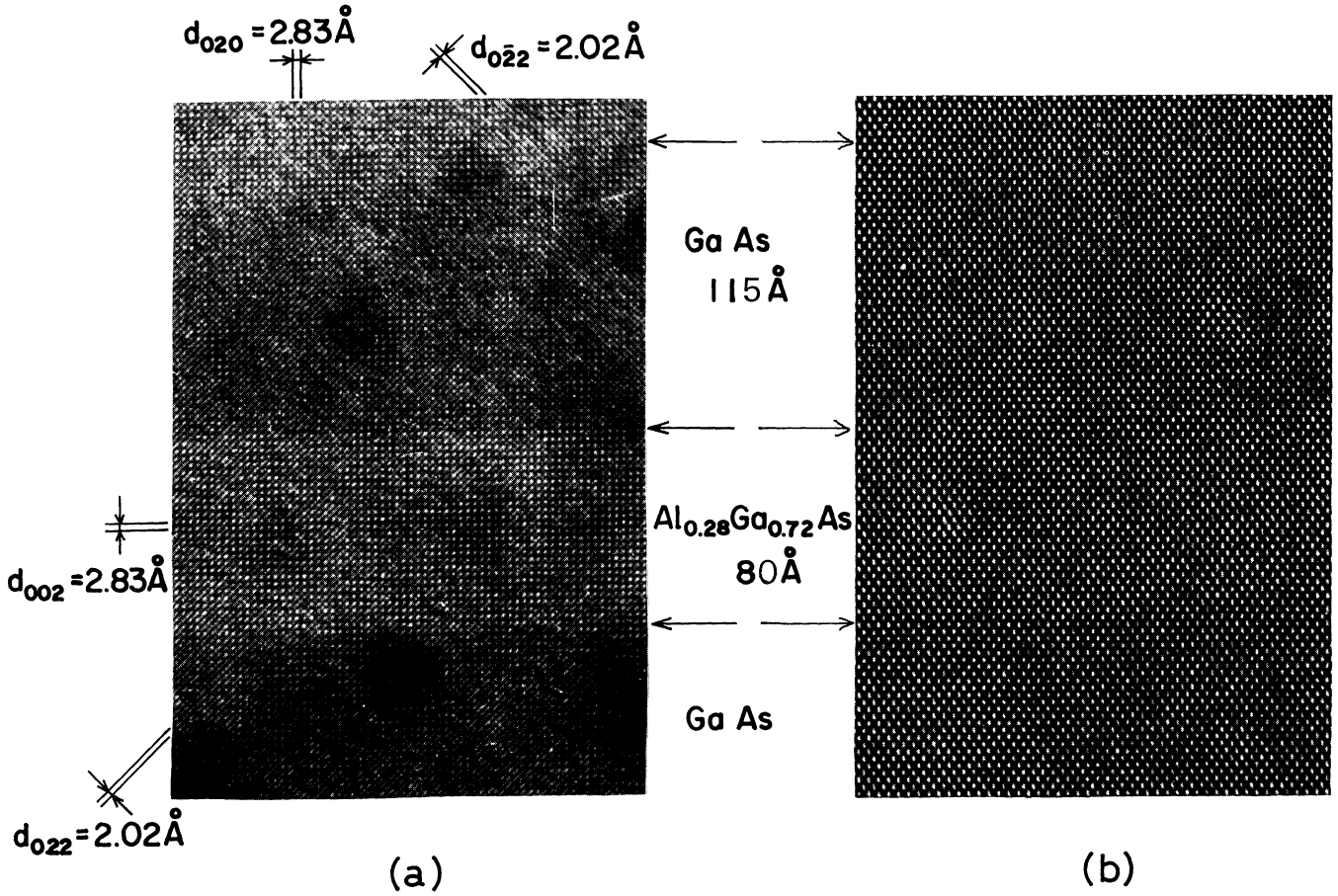

Fig. 3. Cross-sectional lattice image of a GaAs-$Al_{0.28}Ga_{0.72}As$ QW structure taken by a 400 keV trasmission electron microscope. (a) observed from a [100] direction. (b) observed from a [110] direction.

between two adjacent layers of a QW structure made of GaAs-$Al_xGa_{1-x}As$ ($x \fallingdotseq 0.3$). More recently, Suzuki *et al.*[20-22] reported two methods to obtain a lattice image with contrast high enough to distinguish one layer from the other. The first method requires a QW structure having a large difference (more than 0.45) in Al composition between the QW layer and the barrier layer. In the second method the cross-section from a [100] direction instead of the conventional [110] direction is examined. Although the TEM specimen preparation becomes difficult because the (100) plane is not a cleavage plane, the (100) observation gives a clear contrast even for a QW structure composed of GaAs-$Al_xGa_{1-x}As$ ($x \fallingdotseq 0.3$), which is the most important heterostructure for various device applications. Figure 3 compares the lattice images observed from a [100] direction (a) with that observed from a [110] direction (b). The clear contrast for the former results from the fact that a large number of the 200 and its equivalent diffraction spots, which give rise to the contrast for the GaAs-$Al_xGa_{1-x}As$ QW structure, are involved in the lattice image formation, and that these spots are located as the nearest neighbors of the (000) direct beam spot in the reciprocal lattice plane. The clear contrast was also observed by Hetherington *et al.*[23] From the contrast in the lattice image shown in Fig. 3(a), the roughness at the hetero-interface can be estimated to be not more than one monolayer. It should, however, be noted here that, in order to get more quantitative conclusions, the TEM lattice image observationmust be compared with a computer simulation.

§3. Optical Properties of QW Structure

3.1 *Refractive index*

Figure 4 shows refractive index spectra for four different GaAs-AlAs superlattice structures (solid lines) having different values of L_z and L_B (shown in parentheses) but the same average Al content, $\bar{x}=L_B/(L_z+L_B)=0.55\pm0.03$. The measurement was performed[24] by detecting the reflectance of monochromatic light incident perpendicularly to the superlattice epilayer surface. (The refractive index to be measured is the same as that of the TE mode of the guided wave in the QW layer, because the electric vectors in both configurations are in the plane of the QW layer. On the other hand, the electric vector of the TM mode of the guided wave is perpendicular to the plane and its refractive index is in general different from that obtained in perpendicular incidense because of the stractural anisotropy.) Figure 4 clearly demonstrates that the refractive index of a superlattice is not determined only by $\bar{x}$, but depends strongly on the structural parameter such as L_z and L_B. This is in marked contrast to the random alloy $Al_xGa_{1-x}As$ where the refractive index curve is uniquely determined for a given value of x. A more precise measurement showed that the superlattice with L_B smaller than 4.5 nm has a dispersion curve similar to that for a random alloy $Al_{0.55}Ga_{0.45}As$ (shown by a dotted line), and that a superlattice with L_B greater than 4.5 nm exhibits a dispersion curve which is in-

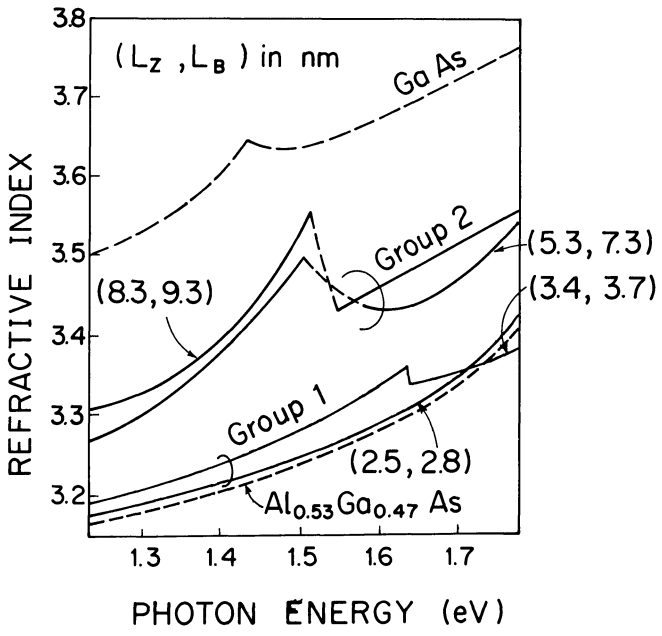

Fig. 4. Refractive index spectra for four different GaAs–AlAs superlattice structures (solid lines) having different values of QW layer thickness L_z and barrier layer thickness L_B (shown in parentheses) but the same average aluminum content $\bar{x}=L_B/(L_z+L_B)=0.55\pm0.03$. For comparison, refractive index spectra for bulk GaAs and for random alloy $Al_{0.55}Ga_{0.45}As$ are shown by broken and dotted lines.

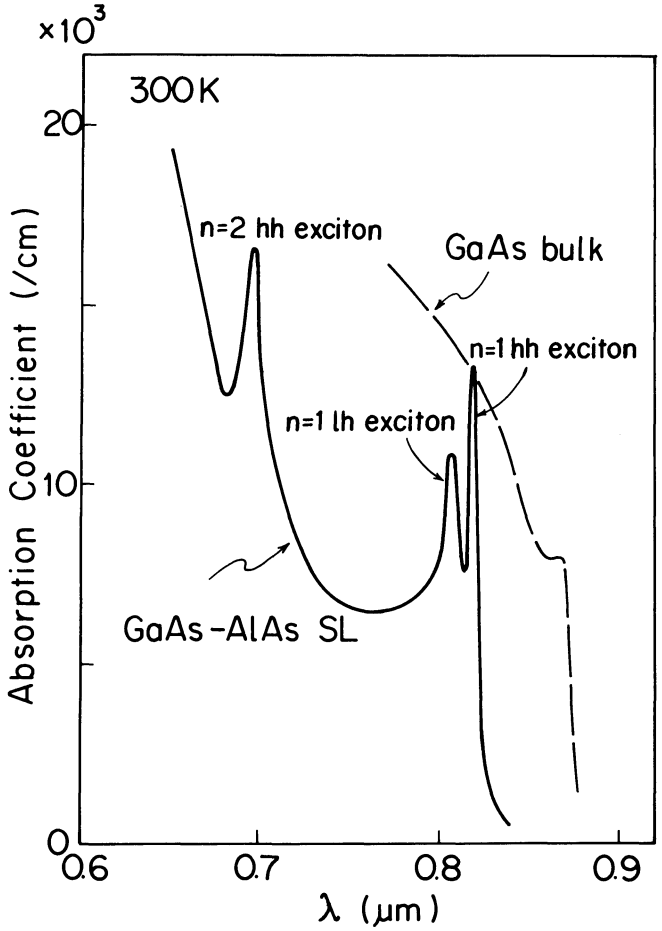

Fig. 5. Optical absorption spectrum measured at 300 K for a GaAs(8.3 nm)–AlAs(9.3 nm) superlattice (solid line). Optical absorption spectrum for high purity bulk GaAs is also shown for comparison (broken line).

termediate between bulk GaAs (shown by a broken line) and the random $Al_{0.55}Ga_{0.45}As$ alloy. This result means that mutual coupling between adjacent QW layers determines the value of the refractive index. Another feature of the superlattice is that the refractive index at the effective bandgap energy, at which a cusp appears in the dispersion curve, differs by as much as 0.2 to 0.3 from that of bluk GaAs. This is in marked contrast to the random alloy $Al_xGa_{1-x}As$, where the refractive index at the bandgap energy does not depend upon x.[25] The refractive index at the bandgap energy is especially important for the design of MQW laser diodes and waveguides. The two features described for the refractive index have been successfully applied to advanced versions of MQW laser diodes, the typical examples of which will be described in §4.2.1.

3.2 *Optical absorption*

The optical absorption spectrum of a QW structure has a staircase shape reflecting the two-dimensional density-of-states $\rho(E)$. This is in marked contrast to the parabolic shape of the absorption spectrum for bulk crystals. A more strinking feature, however, is the existence of exciton absorption peaks which appear at the edge of each step of the staircase for the QW structure. Therefore, discussion in the following subsection is mainly concerned with the exciton and its related physics.

3.2.1 *Room-temperature exciton*

Figure 5 shows an optical absorption spectrum at 300 K for a GaAs–AlAs QW structure (solid line).[4] At the step-edge energies for $n=1, 2, 3\cdots$electron to heavy- and light-hole transitions, a double peak structure appears. This double peak structure does not change in a temperature range from cryogenic temperature, where the peaks have been assigned to excitons,[2] to room temperature,[4] so that it is referred to as room-temperature exciton. More recently, the double peak structure was reported to be preserved even to temperature as high as 473 K or more.[26] This is in marked contrast to bulk GaAs where excitonic absorption peak appears predominantly at lower temperatures. At room-temperature a vanishing trace appears as a shoulder at the absorption edge only for high purity epitaxial GaAs films (broken line). After the first observation in 1981, the room-temperature exciton has been found in a variety of material systems, which are GaAs–$Al_xGa_{1-x}As$ QW structure reported by Miller *et al.*[27,28] in 1982, $Ga_{0.47}In_{0.53}As$–$Al_{0.48}In_{0.52}As$ QWs reported by Wood *et al.*[29,30] in 1984, and GaSb–$Al_xGa_{1-x}Sb$ QWs reported by Miyazawa and his co-workers[31] in 1985.

Already in 1966, Shinada and Sugano[32] predicted that in the limit of two-dimensionality ($L_z\to0$), the spatial extent of the exciton wavefunction is shrinked, and then, the oscillator strength and binding energy of the free exciton is enhanced by a factor of 8 and 4 as compared to the three-dimensional exciton. As for the oscillator strength, Matsuura and Shinozuka[33] reported in 1984 a calculation by a variational method for more realistic

QW structures. The calculation took into account the increase in the density-of-states of the ground level due to the reduction of L_z. Their results were confirmed by Masumoto *et al.*[34] Figure 6 shows that the integral intensity of the $n=1$ heavy-hole exciton absorption peak, which is proportional to the oscillator strength, increases when reducing the QW layer thickness L_z. This increase is much stronger than the $(1/L_z)$ dependence (broken line) which reflects the change of the density-of-states.

Measurements of the binding energy of the two-dimensional exciton were first tried by Miller *et al.*[35] using photoluminescence excitation spectroscopy. They attempted to observe the excited state (2 s state) of the exciton, but no distinct separation of this state from the edge of the band continuum was obtained, which led to an erroneous result in determination of the binding energy. Later, Tarucha *et al.*[36] and Maan and his co-workers[37] measured the binding energy by a band-to-band magnetoabsorption method at 4.2 K. In this case, the optical absorption spectrum was measured under a high magnetic field applied perpendicularly to the plane of the QW wafer. Electrons and holes are then in quantized Landau orbitals, and optical transitions from valence band Landau levels to conduction band Landau levels with equal Landau number l become allowed (i.e. $\Delta l=0$). Therefore, the optical absorption spectrum consists of a series of peaks corresponding to different Landau levels. The peak energy in these Landau level transitions increases in proportion to the applied magnetic field. The straight lines for the transition energies as a function of magnetic field for different Landau numbers converge to an energy at zero magnetic field. This energy is equal to the effective bandgap energy for the QW structure. On the other hand, the exciton absorption peak increases, especially in the low magnetic field region, in proportion to the square of the applied field, which is referred to as diamagnetic shift. The exciton peak energy extrapolated to zero magnetic field and subtracted from the effective bandgap energy, gives the exciton binding energy E_{ex}^{B}. The advantage of this measuring method is that the effective bandgap energy can be determined precisely to within an error of ± 1 meV. Figure 7 shows an example of optical absorption spectra for a GaAs(11.2 nm)–AlAs(6.4 nm) MQW structure measured under different values of applied magnetic field. It is important to note that the minimum optical absorption coefficient between adjacent peaks becomes zero under high magnetic field. This is due to the three-dimensional confinement of the carrier system. In contrast to the QW structure, the absorption spectrum for bulk (thick) GaAs films, which is shown in the inset of Fig. 7, never exhibits a transparent band even under higher magnetic fields. This is because carrier confinement is only two-dimensional in this case.

The binding energy of the 1 s state of the heavy-hole exciton is shown in Fig. 8 as a function of the QW layer thickness L_z. The experimental data measured by the described method are denoted by closed circles. When increasing the two-dimensionality (i.e., reducing L_z), the

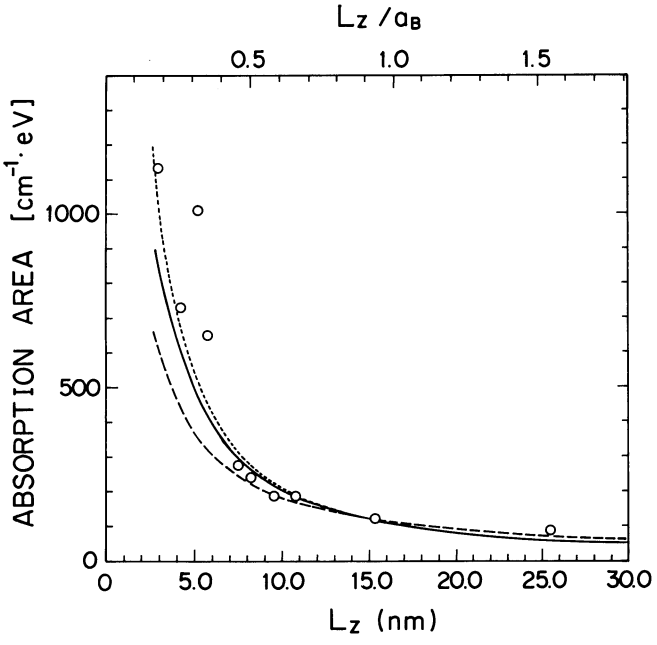

Fig. 6. Absorption area, which is proportional to the oscillator strength, of $n=1$ heavy-hole exciton in GaAs–AlAs quantum-well structure as a function of the QW layer thickness L_z. The broken line shows $1/L_z$ dependence reflecting the density-of-states for the $n=1$ level. Solid and dotted lines are calculated curves by variational method.[34]

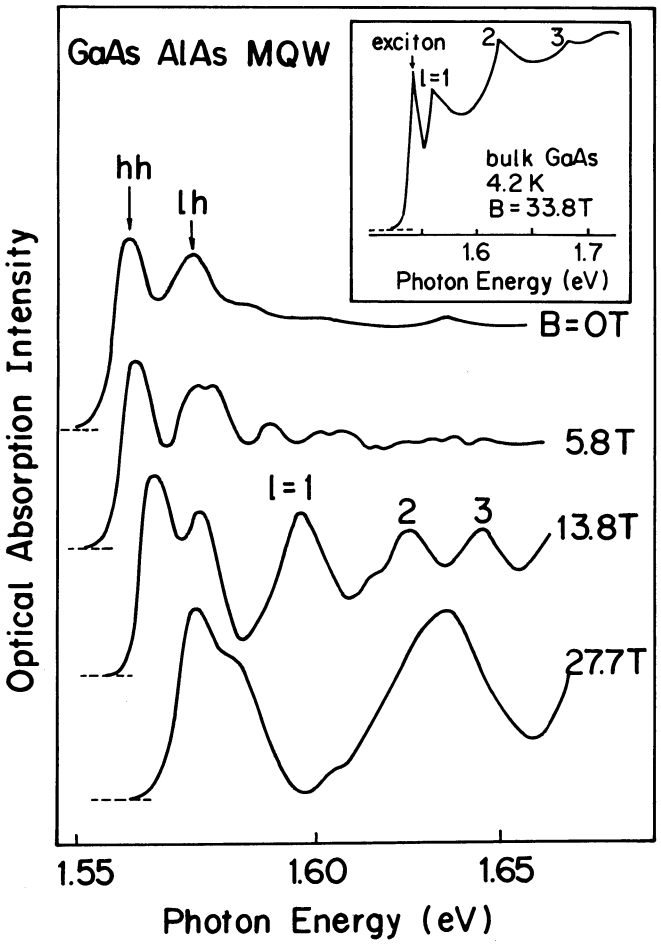

Fig. 7. Magnetic field dependence of optical absorption spectrum for a GaAs(11.2 nm)–AlAs(6.4 nm) MQW structure measured at 4.2 K. hh and lh indicate the $n=1$ heavy-hole and light-hole exciton peaks. Band-to-band Landau level transitions are indicated by $l=1, 2, 3, \cdots$. Inset is an optical absorption spectrum for bulk GaAs at 33.8 Tesla.

binding energy increases from the value of 4.2 meV in bulk GaAs to 15 meV at $L_z=5.8$ nm. The present experimental data are 2–3 meV larger than those obtained from the photoluminescence excitation spectrum measurement performed by Miller *et al.*[35] (shown by dotted line), but agree reasonably well with the variational calculation (shown by a solid line) done by Iwasa**) assuming the reduced mass of $\mu=0.058\,m_0$ which is almost the same value as that reduced from the electron and the heavy-hole effective masses in bulk GaAs.

The diamagnetic energy shift ΔE_d is expressed by

$$\Delta E_d=\langle\phi|\gamma^2(x^2+y^2)/4|\phi\rangle=\eta B^2 \qquad (3)$$

where $\gamma=e\hbar B/(2\mu cR)$ is the magnetic field normalized by using the reduced mass μ and the effective Rydberg R, while η is a diamagnetic coefficient. η expresses the spatial extent of broadening of the exciton in the x–y plane. Figure 9 shows the diamagnetic coefficient η for $n=1$ heavy-hole excitons (open circles) and light-hole excitons (solid circles) in QW structures as a function of the QW layer thickness L_z. η reduces as L_z decreases, which means the shrinkage of exciton wavefunction in the x–y plane. The data for the heavy-hole excitons lie well upon a calculated curve (broken line) assuming the reduced mass of $\mu=0.0583m_0$ again. On the other hand, an agreement between the experimental data for the light-hole exciton and the calculation is obtained only when the assumption of a rather large value of the reduced mass of $(0.09\text{–}0.15)\times m_0$ for the light-hole exciton is made, which reflects the complexity in the $E-k$ relationship in the valence band of the QW structure. This complexity is now under investigation by many researchers.

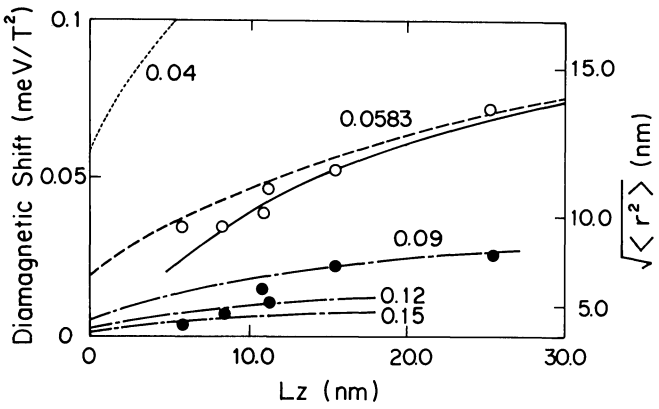

Fig. 9. Diamagnetic coefficient η defined by equation (3) in the text, which is the spatial extent $\sqrt{\langle r^2\rangle}$, of $n=1$ heavy-hole exciton (open circles) and light-hole exciton (closed circles) as a function of the QW layer thickness L_z. Different curves are calculate ones assuming different values of the reduced mass μ indicated on each curve.

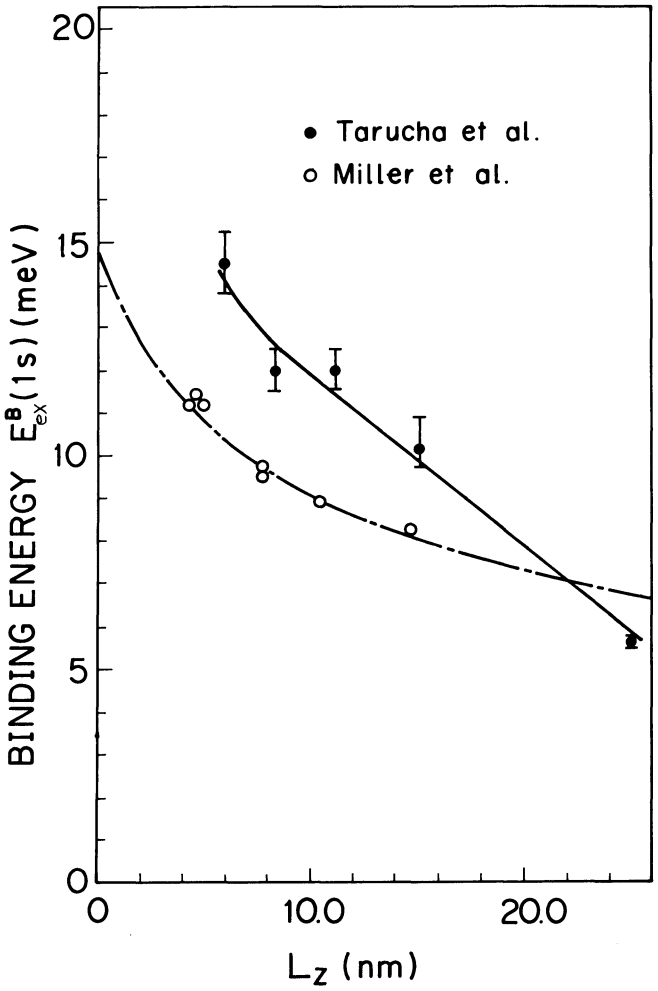

Fig. 8. Binding energy of the 1 s state of $n=1$ heavy-hole exciton as a function of QW layer thickness L_z. Solid circles are measured by magnetoabsorption method.[36] Solid line is calculated by assuming the reduced mass $\mu=0.058m_0$.** Dotted line is the result obtained by photoluminescence excitation spectrum measurement.[35]

The magnetoabsorption method was also applied to $Al_xGa_{1-x}As$(10 nm)–AlAs QW structures.[38] In these structures, the QW layer is composed of the ternary alloy $Al_xGa_{1-x}As$. In spite of the microscopic compositional inhomogeneity inherent to the random alloy, the room-temperature exciton was observed up to a composition $x=0.41$ which is almost equal to the composition at which the direct-to-indirect crossover occurs. The binding energy of the exciton increases with increase in the Al composition x in the QW layer. It is 12 and 20 meV for $x=0$ and $x=0.4$, respectively.

3.2.2 *Optical non-linearity associated with room-temperature exciton*

In 1982, Miller *et al.*[27,28] demonstrated that a reduction of the absorption coefficient (usually noted as the absorption saturation) at the exciton resonance energy takes place at an optical intensity nearly 10 times lower than that required for bulk GaAs or even for the band-to-band transition in the QW structure. The physical reason why the QW exciton absorption can saturate more easily is that this saturation is due to screening of excitons by free carriers—a mechanism qualitatively different from the filling of conduction and valence band states in the bulk GaAs. More precise measurements were done at 2 K by Masumoto *et al.*,[39]*** the result of which is shown in Fig. 10. This figure shows the absorption spectrum at different levels of the measuring light intensity. Especially important in this figure is that the decrease of the absorption coefficient is prominent not exactly at the exciton peak but on its skirt on the long wavelength side.

**Y. Iwasa, private communication.

***S. Tarucha *et al.* private communication.

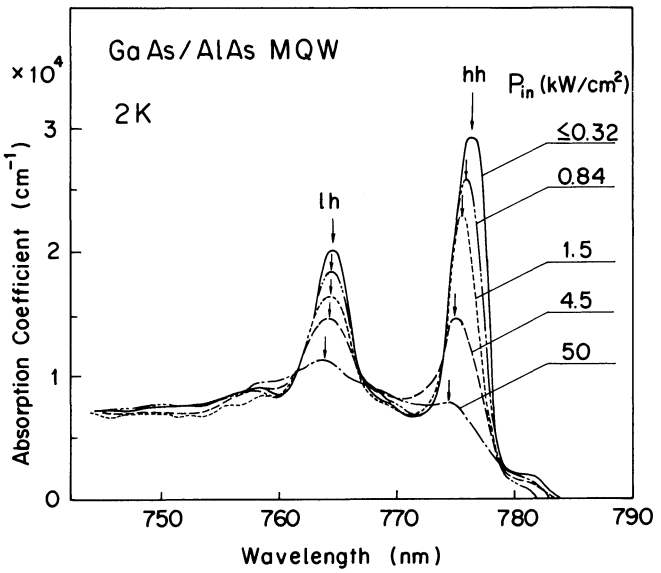

Fig. 10. Optical absorption spectrum measured at 2 K for GaAs-AlGaAs MQW structure with different levels of measuring light intensity P_{in}. hh and lh are the $n=1$ heavy-hole and light-hole excitons, respectively.***

This may be related to the saturation by generated excitons of the lower energy side of the excitonic states, which are localized in thicker areas of the QW layer whose thickness is inhomogeneously distributed due to the monolayer thickness variation described in §2. Degenerate four wave mixing measurement is a method to measure the nonlinear optical interaction between an intense pump laser pulse and a weak probe with the same wavelength, and by using this method Chemla *et al.*[40] revealed the whole aspect of the exciton related optical non-linearity not only for the absorption coefficient bu also for the related refractive index.

3.2.3 *Electric field effect of exciton*

The effect of an electric field applied perpendicular to a QW layer was first studied in 1982 by Mendez *et al.*[41] They observed a decrease of the PL intensity by increasing the reverse bias voltage applied to a Schottky junction made of a metal and a QW structure. Soon after this, Bastard *et al.*[42] established a theory of the electric field effect in a QW structure, which interprets many aspects of electric field effect other than the drastic decrease in PL intensity. According to this theory, the $n=1$ quantized energy level E_1 in the QW layer decreases under a perpendicular weak electric field F ($eFL_z \ll (\hbar^2/2m^*)\times(\pi/L_z)^2$) by an amount equal to

$$\Delta E_1 = 2.2\times10^{-3}\times(m^*e^2/\hbar^2)\times F^2L_z^4 \quad \text{(eV)} \qquad (4)$$

This equation shows that the energy shift ΔE_1 is larger for a larger QW layer thickness L_z. Therefore a compromise exists between the large electric field effect and the two-dimensionality. Values of $L_z=5$–15 nm are appropriate for the co-existence of the two phenomena. Wood *et al.*[43] measured a p-i-n DH diode where an intrinsic (i) MQW layer is sandwiched by p-type and n-type $Al_xGa_{1-x}As$ clad layers, and found that the exciton absorption peak in the MQW layer shifts to lower energy side by increasing the electric field. They demonstrated an ultrafast (131 ps) optical intensity modulator[44] by using this effect. The exciton peak energy shift can be well explained by the equation (4) if a small correction for the binding energy of the exciton is made. Although the electric field effect on the optical absorption in the QW structure is, in general, analogous to the electroabsorption effect (Franz-Keldysh effect) in a bulk material, it is distinct in the following three aspects, all of which are associated with the exciton.

(1) An electric field can control the energy of the large absorption peaks at the bandedge due to excitons which is stable at room-temperature.

(2) By increasing the electric field, the exciton peaks shift with some broadening, but the peaks are not extinguished even at very high fields exceeding 1×10^5 V/cm.[45-49] In other words, the carrier confinement in the QW layer prevents excitons from the electric field induced ionization. This is the reason for the electric field effect in the QW structure being referred to as the Quantum Confined Stark Effect (QCSE).[45-48]

(3) An electric field deforms the square shaped potential well so as to localize electrons at one edge of the well and holes at the opposite edge, thereby changing the selection rule for optical transitions in such a way that forbidden transitions $\Delta n \neq 0$ become observable.[50] The forbidden exciton peaks in the absorption spectrum allow a precise measurement of the energy separation between the ground level and the higher order levels of the conduction band, from which we can determine the conduction band offset in the QW structure.[49]

Usually, the optical absorption spectrum under an electric field is measured in a p-i-n DH diode consisting of an intrinsic (undoped) MQW structure, where a part of the substrate is etched off to avoid light absorption. Recently, it became evident[51] that the spectrum of the photocurrent flowing out of the diode is a replica of the real absorption spectrum of the intrinsic MQW layer. Figure 11 is a typical example of the photocurrent spectrum, the parameter being the applied bias voltage. In this figure, the $n=1$ heavy-hole and light-hole excitons are clearly shown to undergo the long wavelength shift with some broadening by increasing the bias voltage in the reverse direction. If the light wavelength is fixed at or beyond the absorption edge and the bias voltage is increased in the reverse direction, then the photocurrent peak appears at the bais voltage where the exciton peak energy coincides with the incident light wavelength. Therefore, a double peak structure due to the $n=1$ heavy- and light-hole excitons appears in the I–V curve of the diode. The photocurrent peak accompanies, as a matter of fact, a negative resistance region in the I–V characteristics. This photo-induced negative resistance is the basic principle for new optical devices named as self-electrooptic effect device (SEED)[45] and its related devices.[47]

All electric field effects described above are related to the perpendicular electric field effect. As for the parallel electric field effect where the electric field is applied in the plane of the QW layer, the long-wavelength shift was also observed by Chemla *et al.*[52] in 1983. But, since then, there have been no reports. The reason is probably due to

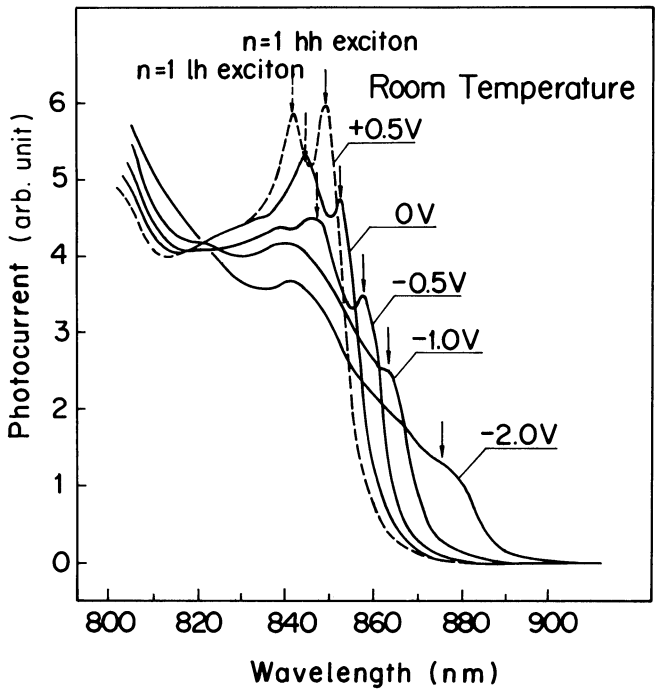

Fig. 11. Photocurrent as a function of wavelength of light incident on a p-i-n DH diode with i-region composed of an MQW structure. Electric field strength corresponding to bias voltage is 6×10^4 V/cm for 0 V and 1.5×10^5 V/cm for -2.0 V.

the technological problem in applying parallel electric field uniformly.

§4. QW Laser Diode

A QW laser diode (LD) is a DH LD whose active layer includes a QW structure, in contrast to a conventional DH LD whose active layer is so thick (more than 50 nm) that no quantum size effect is expected. The family of QW LDs comprises many versions depending on the number of the QW layers, including as a multi-quantum-well (MQW) LD, a single-quantum-well (SQW) LD etc.

The first demonstration was achieved by van der Ziel *et al.*[53] in 1975, but with a limited success because of the immaturity in the epitaxial technology. In the following work by Holonyak's group, it was reported that the threshold current density J_{th} of an MQW LD is less sensitive to the ambient temperature change (larger characteristic temperature T_0 where T_0 is expressed in $J_{th}\propto\exp(T/T_0)$) than the conventional DH LD.[54] Furthermore, these authors raised the interesting speculation[55] that an LO-phonon contribution produces the Stokes shift of the lasing energy from the bandedge energy which is the $n=1$ electron to heavy-hole transition energy. A large impact was given in 1981 by Tsang[56] who realized an MQW LD having J_{th} lower by a factor of three than the minimum value for a conventional GaAs DH LD. More recently, a maximum light output exceeding 2 W[57] and 10 W[58] becomes available from a multi-stripe type of an MQW LD in DC operation at 300 K.

In the following, the features specific to a QW LD is described in comparison with a conventional DH LD. The material system is GaAs–AlGaAs except when otherwise noted. This is followed by some results on recent advances in the QW LD.

4.1 *QW Laser diode in comparison with conventional DH laser diode*

4.1.1 *Low threshold current density*

As described above, QW LDs exhibit J_{th} lower by a factor of three than a conventional DH LD.[56] This is explained by the staircase density-of-states $\rho(E)$ which is favorable to achieve a narrow bandwidth of the optical gain with high peak value as compared to the parabolic density-of-states in a conventional DH LD.

4.1.2 *Large T_0 value*

MQW LDs were reported to have T_0 larger than the conventional DH LD.[54,59] This was explained in terms of the staircase density-of-states $\rho(E)$ which makes the energy distribution of carriers less temperature-sensitive.[60,61] This feature becomes significant in long-wavelength ($\lambda=1.3$–1.5 μm) LDs, since the conventional DH LD made from $Ga_xIn_{1-x}P_yAs_{1-y}$-InP has a small value of T_0 such as 60 K. Very recently, T_0 equal to 160–180 K was indeed reported for $Ga_xIn_{1-x}P_yAs_{1-y}$-InP MQW LDs with relatively thick QW layers grown by conventional liquid phase epitaxy (LPE),[62-64] or vapor phase epitaxy (VPE).[65]

4.1.3 *Polarization dependent optical gain*

In the QW structure, a TE polarized optical wave whose electric vector lies in the plane of the QW layers can couple both with the electron to heavy-hole transition and with the electron to light-hole transition, but a TM polarized optical wave whose electric vector is perpendicular to the plane of the QW layers is allowed to couple only with the latter transition, so that the optical gain for the TE wave is much larger than for the TM wave since the $n=1$ heavy-hole energy level is lower and has larger density-of-states than the $n=1$ light-hole energy level.[66-68] An optical gain measurement by Kobayashi *et al.*[69] showed that gain difference at threshold between the TE and TM waves is as much as 120 cm^{-1} for an MQW LD, while it is at most 20 cm^{-1} for the conventional DH LD. This large anisotropy in optical gain for the MQW LD guarantees that the LD oscillates selectively with the TE polarization. The significance of this anisotropy or selectivity becomes clear when we remind ourselves of the currently well developed distributed feedback (DFB) LD for use of the optical communication. In this type of LD, there is no function provided for selecting polarization, so that small perturbation such as ambient temperature makes the oscillation unstable in polarization.[70] An MQW-DFB LD was demonstrated very recently by Dutta *et al.*[71] at $\lambda=1.5$ μm using LPE.

4.1.4 *Stability in oscillation wavelength*

An MQW LD is narrower in optical gain spectrum width due to the staircase density-of-states $\rho(E)$ than the conventional DH LD, so that the former is easier to oscillate in a single longitudinal mode (single wavelength oscillation) than the latter. This was confirmed experimentally by comparing the two types of the diodes under direct current modulation at high bit rate.[72] Recently, Uomi *et al.*[73] reported that the maximum frequency for the direct modulation exceeds 10 GHz in an MQW LD, which is higher by a factor of two as compared with the conventional DH LD.

4.1.5 *Reduced chirping*

Chirping is a shift of the lasing wavelength resulting from the change of the refractive index due to a modulation of the injected carrier density. Dutta *et al.*[74,75] reported that the chirping is smaller by a factor of three in an MQW LD than in a conventional DH LD. This was furthermore confirmed by Toba *et al.***** by comparing an MQW LD made from GaSb-AlGaSb with a conventional $In_xGa_{1-x}P_yAs_{1-y}$-InP DFB LD operating at $\lambda=1.5\,\mu m$.

4.1.6 *Low loss in a waveguide at the lasing wavelength and its implication in monolithic integration*

Figure 12 shows absorption loss spectra for an MQW waveguide (solid line) and for a conventional DH waveguide (broken line) under no current injection. Due to the staircase density-of-states $\rho(E)$ for the MQW structure, the absorption loss changes more steeply at the bandedge in the former waveguide as compared to the latter one. When both types of waveguide are current-injected, spontaneous emission and laser oscillation start at wavelength λ_{sp} and λ_{LD}, respectively. For both waveguides, a long wavelength shift $(\lambda_{LD}-\lambda_{sp})$ corresponding to 20–30 meV in energy occurs due to the bandgap shrinkage effect which will be described in §4.1.7. Important is that optical absorption at the lasing wavelength λ_{LD} is much smaller in the MQW waveguide than in the conventional DH waveguide.[76,77] For application significance, this implies that, when we consider a monolithic integration of an LD with other passive waveguide elements, the absorption loss of the passive waveguide element at the wavelength of the LD becomes small. Monolithic integration of an MQW LD with a waveguide modulator making use of the electric field effect of the room-temperature exciton, as first demonstrated by Tarucha *et al*,[78] will be described in Section 5.

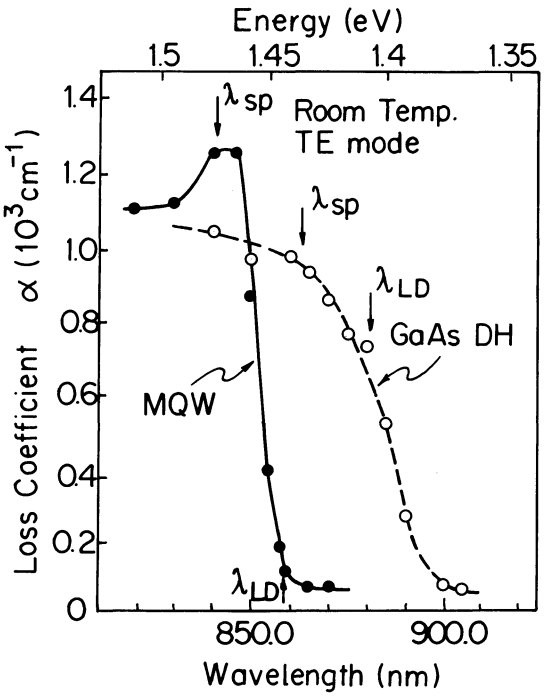

Fig. 12. Absorption spectrum for an MQW waveguide (solid line) and for a conventional GaAs DH waveguide (dashed line) under no current injection. λ_{sp} and λ_{LD} are wavelengths for spontaneous emission and laser oscillation, respectively, when current is injected into the waveguide.

4.1.7 *Bandgap shrinkage*

Using photo-pumped laser oscillation, Holonyak *et al.*[55] found that there are two luminescence peaks, one corresponding to the $n=1$ electron to heavy-hole transition (bandedge luminescence), the other being located at an energy lower by 20–40 meV than the bandedge. The laser oscillation occurred at the latter peak, which was ascribed to an LO-phonon participation. Subsequent work by Tarucha *et al.*,[66,79,80] however, denied the LO-phonon model, and clarified (1) that the double peak structure originates from an artifact of a single luminescence peak passing through a waveguide whose absorption spectrum has a staircase shape, and (2) that the lower energy peak is due to bandgap shrinkage induced by an increase of the injected carrier density n. Its energy separation ΔE from the bandedge increases with n following the relationship $\Delta E \propto n^{1/m}$ $(m=2.7\text{–}3)$ which represents the bandgap shrinkage effect well known for bulk material.[81]

4.2 *Recent advances in QW laser diodes*

4.2.1 *QW laser diodes fabricated by compositional disordering*

Compositional disordering is a material modification technology, which will be described in detail in §6. When impurity diffusion or ion-implantation is performed, a superlattice changes to a random alloy crystal losing the periodicity characteristic of the superlattice. The resultant random alloy differs in bandgap energy and optical refractive index from the original superlattice.

Application of this material modification technology to device fabrication was first reported by Holonyak *et al.*[82] for demonstrating an MQW LD integrated with an external cavity. Later, Fukuzawa *et al.*[83] reported a buried MQW LD which ensures the lateral mode stability. Suzuki *et al.*[84] demonstrated a window-stripe MQW LD, by which the ultimate output light power level is increased by a factor of three.

4.2.2 *Visible QW laser diode*

To explit the short wavelength light emission limit in the QW structure composed of the Al-Ga-As material system, two different approaches are considered. One is to utilize the binary-well QW structure where the QW layer is made from GaAs. When this layer thickness L_z decreases, the quantum energy levels for electrons and holes increase, thereby increasing the light emission energy. The other approach utilizes the ternary-well QW structure where the QW layer is from ternary $Al_xGa_{1-x}As$ alloy. When the Al content x is increased in this layer while keeping its thickness L_z constant at, for example, 10 nm, the bottom of the potential well is raised, thereby also increasing the quantum energy levels for electrons and holes.

Figure 13 shows a comparison[85] between the binary-well and the ternary-well MQW structures. Here the relative PL intensity at 300 K is plotted as a function of the PL peak energy (wavelength). In the binary-well MQW, the PL intensity starts to decrease around $\lambda=720$ nm,

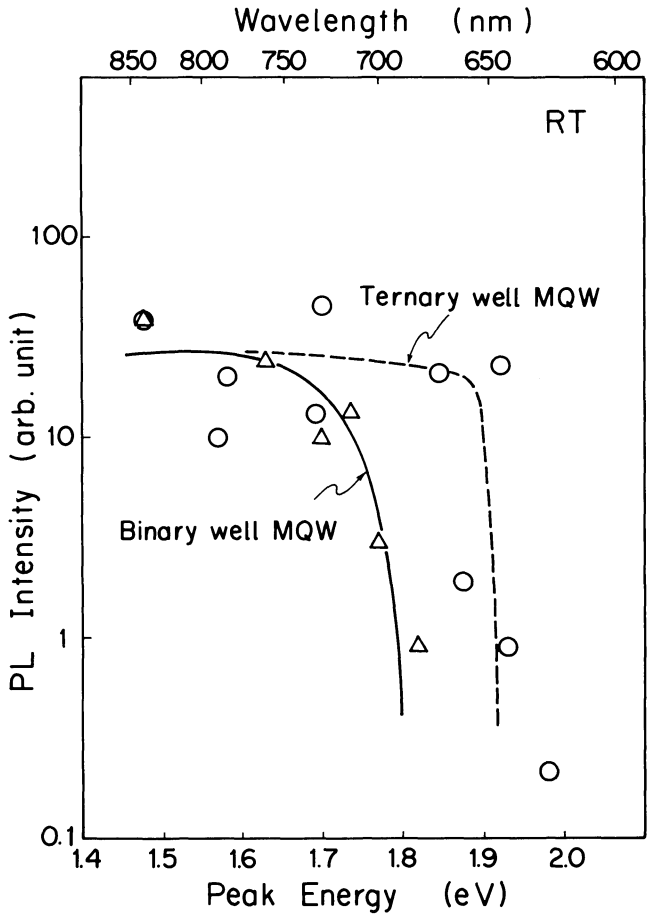

Fig. 13. Photoluminescence intensity at 300 K as a function of the photoluminescence peak energy (wavelength) for binary(GaAs)-well MQW structure and for ternary ($Al_xGa_{1-x}As$)-well MQW structure.

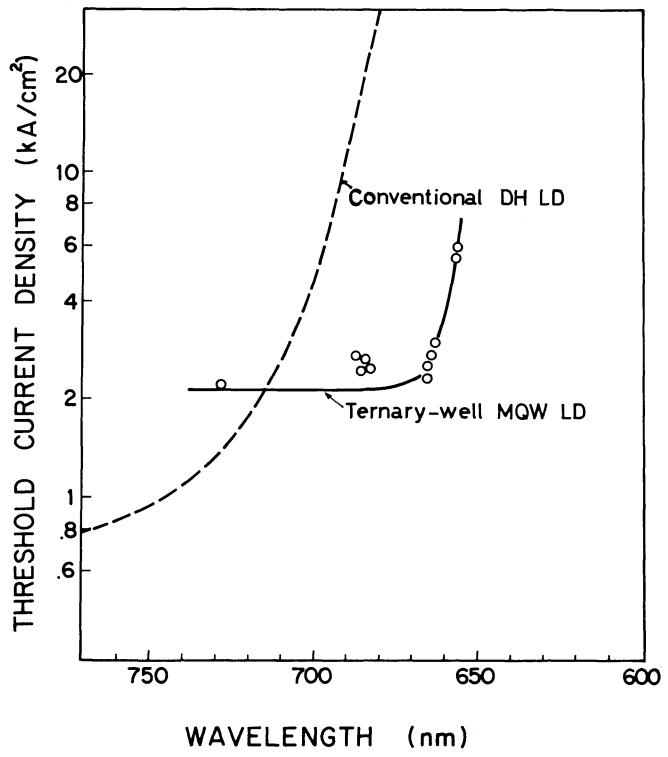

Fig. 14. Threshold current density at 300 K as a function of lasing wavelength for ternary($Al_xGa_{1-x}As$)-well MQW laser diode (solid line), in comparison with the best data reported so far for the conventional DH laser diode with $Al_xGa_{1-x}As$ active layer (broken line).

while in the ternary-well MQW, it is kept almost constant down to $\lambda = 650$ nm. The PL intensity decrease is usually explained in terms of the band-crossover in the conduction band in which the $n=1$ quantum level for the Γ electrons comes close to or above the $n=1$ quantum level for the indirect band electrons (L or X electrons). The reason for the difference in PL intensity drop between the binary-well and the ternary-well MQWs described above is not clear, but it may be related to the problem of the conduction band discontinuity (ΔE_c) in these QW structures.

MQW LDs having the ternary-well MQW active layer can lase up to a wavelength much shorter than the conventional DH LDs with ternary $Al_xGa_{1-x}As$ active layers.[86] Figure 14 shows J_{th} at 300 K as a function of the lasing wavelength for the ternary-well MQW LDs (solid line) in comparison with the best data so far reported for the conventional DH LDs with ternary active layers (broken line). Iwamura *et al.*[87] demonstrated a continuous operation at $\lambda = 660$ nm near room-temperature by using a ternary-well MQW LD with QW layers composed of $Al_{0.35}Ga_{0.65}As$.

4.2.3 *Long wavelength QW laser diode*

The long wavelength region ($\lambda = 1.3$–$1.6\,\mu$m) is important for optical communication. Intensive efforts to use the advantages in the QW LD described in §4.1 into LDs operating in this wavelength region have been made recently, but at the present stage the results were not always successful. The problem seems to arise from the epitaxial technology. $Ga_xIn_{1-x}P_yAs_{1-y}$ is the most versatile material system. However, for accurate lattice matching, this material requires a strict control of compositions x and y to within ± 1 percent. The conventional MBE technology cannot provide the control of two species of the rather volatile group V elements. In order to overcome this shortcoming, the gas source MBE was proposed by Panish *et al.*,[88] which was successful to fabricate a conventional DH LD. But even with this technology no report has been published concerning 300 K continuous operation of a QW LD. Although the 300 K continuous operation was reported for an MQW LD fabricated by using a modified version of the conventional LPE[62-64] or VPE,[65] the minimum layer thickness realized with these technologies is limited to 15 nm or so, which is not thin enough to expect the room-temperature exciton effect described in §3.2.

The second candidate is the $Ga_{0.47}In_{0.53}As$–$Al_{0.48}In_{0.52}As$ material system which contains only one species of the group V element. Although 300 K pulse operation of an MQW LD grown by MBE was reported by Temkin *et al.*[89,90] by MBE, no data were given on the continuous operation.

The third candidate is the GaSb–$Al_xGa_{1-x}Sb$ material system. Ohmori *et al.*[91-93] recently succeeded in realizing 300 K continuous operation of an MQW LD emitting at $\lambda = 1.67\,\mu$m, by carefully controlling the MBE growth conditions.[94] This LD exhibits superior dynamic response compared to the conventional DFB LD.****

****H. Toba and K. Nosu: *Conf. Lasers and Electrooptics, San Francisco, 1986*, ThS4.

Furthermore, the room-temperature exciton was observed in this MQW structure.[31]

§5. Novel Optical Devices Using Room-Temperature Exciton

As described in §3.2, the exciton in the QW structure is stable at room-temperature and, furthermore, it exhibits the large optical non-linearity and the quantum confined Stark effect (QCSE). The unique excitonic features will generate a novel class of optoelectronic devices without a close precedent. These devices will be very important not only for optical communication but also for optical signal processing in optical computers and for optical switching (exchanging) systems.

The first example was an optical bistable switch, in which an MQW epilayer was sandwiched to form a Fabry-Perot etalon.[95] This device was making use of the optical non-linearity associated with the exciton. In the positive feedback scheme of the etalon with non-linear medium, the output optical intensity becomes a multi-valued function of the input optical intensity, thereby giving rise to an optical bistability. In this device, the rise time for an optical pulse was very fast (less than 1 ps), but the fall time was very long (more than 10 ns). This limit was given by the free carrier recombination life time. Recently, an effort was reported to reduce the carrier life time by favorably introducing a surface recombination effect.[96]

Wood *et al.*[43,44] demonstrated an ultrafast (131 ps) modulator of light transmitting perpendicularly to an MQW structure that exhibits the QCSE, as described in §3.2.3. A similar device was demonstrated with a $Ga_{0.47}In_{0.53}As$–$Al_{0.48}In_{0.52}As$ MQW structure for the 1.5 μm wavelength region by Wakita *et al.*[97] A waveguide type QCSE modulator was fabricated by Tarucha *et al.*[98] and independently by Wood *et al.*[99] The latter authors realized very high frequency operation of more than 10 GHz with a modulation depth of 1:10 or more, which is superior to the waveguide modulator utilizing dielectrics, while the former authors reported an advantage for monolithic integration of the QCSE modulator with an MQW laser diode because of the low loss property of the waveguide at the wavelength of a monolithically integrated laser diode.[78]

The self-electrooptic effect device (SEED), which was proposed by Miller *et al.*,[45,47] utilizes the negative resistance in the photocurrent (I_p) versus voltage (V) characteristic resulting from the QCSE in a p-i-n DH diode as explained in §3.2.3. The operation principle of the SEED can be understood in a manner analogous to purely electrical negative resistance circuits such as those utilizing tunnel diodes. The I_p–V curve shifts vertically as a function of incident optical power P_{in}. At some range of P_{in}, the I_p–V curve crosses with a fixed load curve at three different points, two of them being stable operation points while the rest an unstable one. Outside this range of P_{in}, there is only one crossing point, which is a stable operation point. Accordingly, the output optical power P_{out} increases with increase in P_{in} along one operation branch, but is suddenly jumps down to the other operation branch at a critical level of $P_{in}=P_{in,1}$. When decreasing P_{in}, P_{out} remains on the latter branch until P_{in} reaches $P_{in,2}$ which is smaller than $P_{in,1}$. Hereafter it jumps up to the original operation branch. Thus, the P_{out}–P_{in} curve shows a hysteresis, which represents the bistable operation. This device can operate at a very small optical power level such as several tens of μW. Although the speed of the device is limited by the device capacitance and a relatively large load resistance (RC time constant is more than several hundred ns), the switching energy per unit area of the device is as low as several fJ/μm^2.

Operation modes of the SEED other than the bistability have also been proposed. These are (1) optoelectronic oscillation, where both the output light intensity and the applied voltage oscillate because of the unstable operation point associated with the negative resistance I_p–V curve, (2) self-linearized optical modulation and (3) optical level shifting. In the latter two, the device operates in a stable operation regime with a constant current supply. Since the current is in exact proportion to the amount of optical absorption in the device, modulation of the current brings about modulation of the output power P_{out}. The concept of the self-linearized modulation includes a light-by-light inverter, and an incoherent-to-coherent converter.[47]

The non-linear behavior of the exciton absorption was successfully utilized in the mode-locking of a laser diode by Silberberg *et al.*[100,101] In this case, an MQW layer with removed substrate was placed inside an external cavity configuration using a conventional GaAs DH laser with one AR (anti-reflection)-coated facet. Proton bombardment was applied to the MQW layer for reducing the recovery time of the saturated absorption, thereby a continuous train of pulses as narrow as 1.6 ps was obtained with a pulse repetition rate of 2 GHz.

More recently, Tarucha *et al.*[102] demonstrated a bistable MQW laser diode utilizing both the QCSE and the optical non-linearity associated with exciton. As shown in the inset of Fig. 15, the laser diode has a tandem electrode configuration. By injecting current into the electrode A while applying voltage to the electrode B,

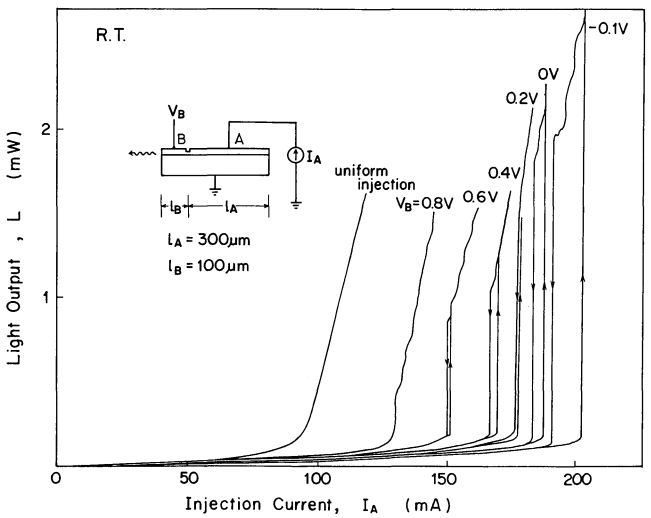

Fig. 15. Light output (L) versus injected current (I_A) characteristics at 300 K for a bistable MQW laser diode with different applied voltage V_B. Inset shows schematic structure of this MQW laser diode with tandem electrode configuration with electrodes A and B.

the light output versus injection current characteristic shown in Fig. 15 exhibits a bistability, which can be controlled by a voltage applied to the electrode B. It is important to note that the applied voltage is lower than the built-in voltage so that no current is injected to the electrode B. This is favorable for low power consumption.

§6. Material Modification Toward Multi-Dimensional Quantum Wells

6.1 *Compositional disordering of superlattices*

The compositional disordering of a GaAs–$Al_xGa_{1-x}As$ superlattice by impurity diffusion or by ion implantation and annealing is very attractive from two points of view as already described in §1 and 4.2.1. Here, the discussion will focus on compositional disordering as a material modification technology, which will introduce a new concept into the field of the material science.

The observation of the compositional disordering was first reported by Laidig *et al.*[7] for a Zn diffused superlattice, followed by Coleman *et al.*[103] for a Si ion implanted superlattice. It was pointed out by Hirayama *et al.*[104] that, when Si ion is implanted into a GaAs–AlAs superlattice, the compositional disordering occurs not during the implantation process but during the subsequent annealing process. This implies that the compositional disordering is not related to the crystal defects introduced during the implantation, which was also confirmed by Kawabe *et al.*[105]

The compositional disordering is caused by the interdiffusion processes of the constituent atoms through heterointerfaces. The interdiffusion process can be detected not only by destructive methods such as Auger electron spectroscopy (AES) or secondary ion mass spectroscopy (SIMS) with simultaneous operation of sputter etching, but also by the non-destructive method of photoluminescence (PL). PL measurements are especially useful to detect the initial stage of interdiffusion. When the square-shaped potential well in the original superlattice is deformed due to the interdiffusion into a shape which is described by using an error function involving an interdiffusion constant D_{int}, the $n=1$ quantum levels for electrons and holes increase, thereby giving rise to a high-energy shift of the PL peak energy. By tracing this energy shift as a function of the lapse of time during annealing, we can obtain the interdiffusion constant D_{int}.[104] D_{int} was found to be independent of the implanted ion dose if the dose is less than 2×10^{14} cm^{-2} for Si ions. This finding also confirms that the disordering is not related to defects.

The implantation of various kinds of ion species, such as Si, F, Ga, As, Be, B, and Ar, into GaAs–AlAs superlattices performed by Hirayama and his co-workers[106,107] has led to the following important conclusions;

(1) Some ion species (Si, Ga, F, As, and B) induce the compositional disordering, while other species (Be and Ar) do not. Especially Ar ions, which act neither as donor nor as acceptor and only induce defects during the implantation, do not induce the compositional disordering at all.

(2) The interdiffusion constant D_{int} is proportional to the diffusion constant D for the ion species in the superlattice, as shown in Fig. 16,

$$D_{int}/D=2\times10^{-4}. \tag{5}$$

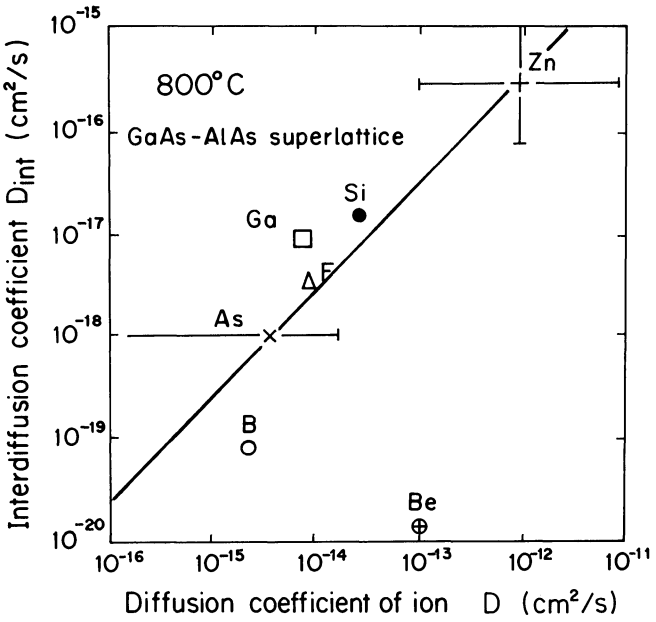

Fig. 16. Interdiffusion constant D_{int} as a function of diffusion constant D for various ion species (Si, Ga, F, As, B, and Be) ion implanted into a GaAs–AlAs MQW structure with subsequent annealing at 800°C. An experimental point for Zn diffusion at lower temperature is also plotted for comparison.

This relation is valid for almost all ion species including the constituent elements Ga and As, but except Be which has a very small ion diameter. This relation means that the diffusion is accompanied by a site exchange between the nearest neighbour group III constituent elements. It is of particular important to point out that the implatation of ions of the constituent elements such as Ga and As also induces the compositional disordering[107] and, furthermore, that D_{int} for Ga ions is as large as that for Si ions.[108]

The focused ion beam (FIB) technology, in which ions are ejected from an edge of a fine needle of a liquid metal ion source, focused by an electrostatic lens system into a diameter of 100 nm or less, and scanned by an electric field applied to the lens system is now under development.[109-111] Among the liquid metal ion sources developed so far, the Ga ion source is the most stable one with a lifetime exceeding 1000 hours. Therefore, the Ga ion implantation using this FIB technology provides the totally new concept of *local material modification*, which includes local compositional disordering[107] and local semi-insulating.[112,113]

6.2 *Multi-dimensional quantum-well structure*

The QW structures described above are ultra-thin film multi-layer structures, in which carriers are one-dimensionally confined. Therefore these structures may be called one-dimensional QW structures. When we extend the concept to the other two dimensions, the resultant structure is called a multi-dimensional QW structure. Figure 17 shows these structures and the corresponding density-of-states $\rho(E)$ schematically. In the one-dimensional QW structure (left), $\rho(E)$ is a staircase function of

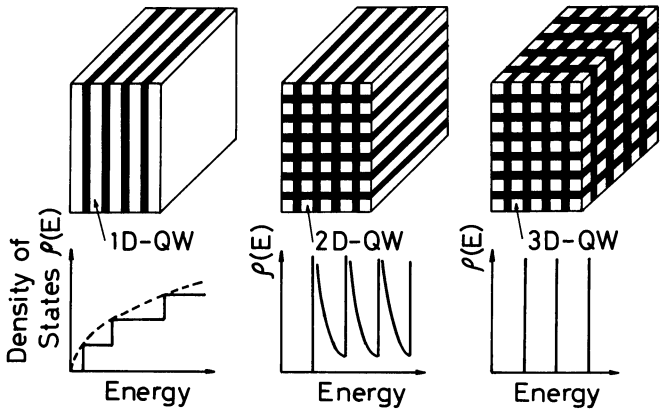

Fig. 17. Multi-dimensional quantum-well structures and their density-of-states $\rho(E)$ as a function of energy.

energy, which is distinct from the parabolic $\rho(E)$ (dashed line) of the bulk material. In the two-dimensional QW structure (center), which is sometimes referred to as a quantum-well-wire (QWW) structure, $\rho(E)$ is a saw-tooth function. In the three-dimensional QW structure (right), which is often named as a quantum-well-box (QWB) or quantum-dot (QD) structure, $\rho(E)$ becomes a train of delta functions. This novel $\rho(E)$ is very attractive for new optical properties, and several theoretical studies[114-117] have already been published.

There is, however, the serious problem of how to fabricate such a fine structure. Petroff *et al.*[118] tried to fabricate a QWW structure with dimension of 20 nm × 20 nm by mesa etching a GaAs SQW or MQW epiwafer and subsequent regrowth. They reported a cathodoluminescence spectrum at low temperature, but this spectrum did not show any feature characteristic to the two-dimensional quantum size effect. Kash *et al.*[119] recently fabricated QWW and QD structures only by mesa etching of a QW epiwafer using a combination of electron beam lithography and reactive ion etching. The minimum dimension of their mesa was 40 nm. Although the mesa was confined by air, an enhancement of the PL intensity at 6 K was observed.

More recently, Ga FIB implantation (acceleration voltage = 100 kV, dose = $2-4\times10^{14}$ cm^{-2}) with line(100 nm)-and-space(200 nm) scan over a GaAs single-quantum-well (SQW) epitaxial wafer surface with subsequent heat treatment (750–800°C, 60 minutes, in H_2 ambient) was used by Hirayama *et al.******) to fabricate a quantum-well-wire (QWW) structure in which a GaAs quantum well is confined not only in vertical direction by the $Al_xGa_{1-x}As$ barrier layers but also in lateral direction by the compositionally disordered $Al_yGa_{1-y}As$ lines. Although the lateral size of this QWW was 150 nm and thus too large to expect the two-dimensional quantum size effect at room temperature, they succeeded in obtaining a photoluminescence spectrum and its excitation spectrum at 4.2 K which clearly exhibits a multiple peak structure resulting from the density-of-states specific to the two-dimensional quantum confinement. Figure 18 shows

*****Y. Hirayama, Y. Suzuki, H. Iguchi, S. Tarucha and H. Okamoto: *Electronic Materials Conf. Amherst 1986*, N-7.

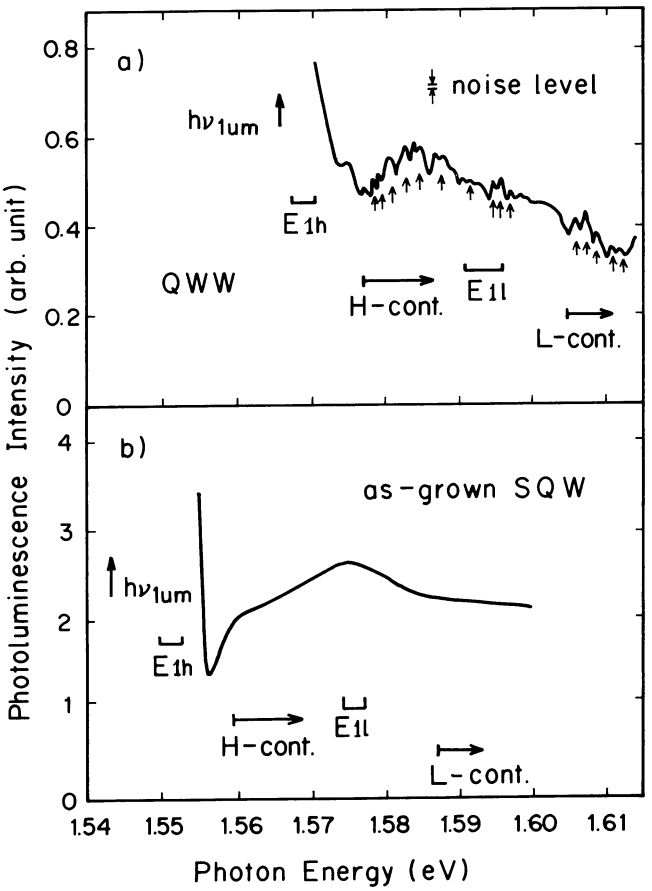

Fig. 18. Photoluminescence excitation spectrum at 4.2 K for a quantum-well-wire (QWW) structure (a) and for a single quantum-well epilayer from which the QWW was fabricated by Ga^+ FIB implantation (b). E_{1h}; heavy-hole exciton energy, E_{1l}; light-hole exciton energy, H-cont.; heavy-hole continuum, L-cont.; light-hole continuum, $h\nu_{lum}$; photoluminescence energy being detected.

a comparison of the photoluminescence excitation spectrum from the QWW structure (a) with the original SQW epilayer from which the QWW was fabricated (b). An independent study of Cibert *et al.*[120] showed a similar multiple peak spectrum from a QWW and a QD which were also fabricated by using the compositional disordering induced by Ga ion implantation.

These two examples represents the first preliminary results. Future progress in nanometer processing technologies combined with epitaxial techniques will generate more fine structures, which will promote the studies on the low-dimensional physics and its applications.

Acknowledgement

The author is indebted very much in preparing this article to the members of the Superlattice Research Group in NTT Electrical Communication Laboratories and to Prof. N. Miura, Dr. Y. Iwasa and Dr. Y. Masumoto, the Institute of Solid State Physics, the University of Tokyo, for the cooperative research on room-temperature exciton, and to Dr. T. Shiokawa and Dr. Y. Aoyagi, the Institute of Physical and Chemical Research, for the technical cooperation in the focused Ga ion beam technology. He wishes to express his thanks to Dr. K. Ploog, Max-Planck Institut für Festkoerperforschung,

Stuttgart, FRG, for critical reading of this manuscript.

References

1) L. Esaki and R. Tsu: IBM J. Res. & Develop. **14** (1970) 61.
2) R. Dingle: *Festkoerperprobleme XV, Advances in Solid-State Physics* ed. H. J. Queisser (Pergamon-Vieweg, Braunschweig, 1975) p. 21.
3) W. T. Tsang: Appl. Phys. Lett. **39** (1981) 786.
4) T. Ishibashi, S. Tarucha and H. Okamoto: *Int. Symp. GaAs and Related Compounds, Oiso, 1984*, Inst. Phys. Conf. Ser. No. 63, Chapter 3 (1982) p. 587.
5) R. Dingle, H. L. Stormer, A. C. Gossard and W. Wiegmann: Appl. Phys. Lett. **33** (1978) 665.
6) T. Mimura, S. Hiyamizu, T. Fijii and K. Nanbu: Jpn. J. Appl. Phys. **19** (1980) L225.
7) W. D. Laidig, N. Holonyak, Jr., M. D. Camras, K. Hess, J. J. Coleman, P. D. Dapkus and J. Bardeen: Appl. Phys. Lett. **38** (1981) 776.
8) *Handoutai Choukoushi no Butsuri to Ohyo* [Physics and Applications of Semiconductor Superlattices] ed. Phys. Soc. Jpn. (Baifukan, Tokyo 1984) [in Japanese].
9) A. C. Gossard, W. Wiegmann, R. C. Miller, P. M. Petroff and W. T. Tsang: *Collected Papers, 2nd Int. Symp. Molecular Beam Epitaxy and Clean Surface Technology, Tokyo 1982*, p. 39.
10) Y. G. Chai and R. Chow: J. Appl. Phys. **53** (1982) 1229.
11) P. M. Petroff, R. C. Miller, A. C. Gossard and W. Wiegmann: Appl. Phys. Lett. **44** (1984) 217.
12) J. J. Harris and B. A. Joyce: Surf. Sci. Lett. **103** (1981) L90.
13) J. H. Neave, B. A. Joyce, P. D. Dobson and N. Norton: Appl. Phys. **A-31** (1983) 1.
14) T. Ishibashi, Y. Suzuki and H. Okamoto: Jpn. J. Appl. Phys. **20** (1981) L623.
15) L. Goldstein, Y. Horikoshi, S. Tarucha and H. Okamoto: Jpn. J. Appl. Phys. **22** (1983) 1489.
16) H. Sakaki, M. Tanaka and J. Yoshino: Jpn. J. Appl. Phys. **24** (1985) L417.
17) T. Fukunaga, K. L. I. Kobayashi and H. Nakashima: Jpn. J. Appl. Phys. **24** (1985) L510.
18) P. M. Petroff: J. Vac. Sci. Technol. **14** (1977) 973.
19) H. Okamoto, M. Seki and Y. Horikoshi: Jpn. J. Appl. Phys. **22** (1983) L367.
20) Y. Suzuki, M. Seki and H. Okamoto: *Extended Abstract 16th (1984 Int.) Conference on Solid State Devices and Materials, Kobe, 1984* (Business Center for Academic Societies Japan, Tokyo, 1984) p. 607.
21) Y. Suzuki and H. Okamoto: Jpn. J. Appl. Phys. **24** (1985) L696.
22) Y. Suzuki and H. Okamoto: J. Appl. Phys. **58** (1985) 3456.
23) C. J. D. Hetherington, J. C. Barry, J. M. Bi, C. J. Humphreys, J. Grance and C. Wood: *Layered Structures, Epitaxy, and Interfaces*, Material Research Society, Symposia Proceedings, vol. 37, eds. J. M. Gibson and L. R. Dawson, 1985 (Material Research Society, Pittsburgh, 1985) p. 41.
24) Y. Suzuki and H. Okamoto: J. Electron. Mater. **12** (1983) 397.
25) H. C. Casey, Jr., D. D. Shell and M. B. Panish: Appl. Phys. Lett. **24** (1974) 63.
26) H. Iwamura, H. Kobayashi and H. Okamoto: Jpn. J. Appl. Phys. **23** (1984) L795.
27) D. A. B. Miller, D. S. Chemla, P. W. Smith, A. C. Gossard and W. T. Tsang: Appl. Phys. **B28** (1982) 96.
28) D. A. B. Miller, D. S. Chemla, D. J. Eilenberger, P. W. Smith, A. C. Gossard and W. T. Tsang: Appl. Phys. Lett. **41** (1982) 679.
29) T. H. Wood, C. A. Burrus, J. S. Weiner, D. S. Chemla, D. A. B. Miller, T. C. Damen, D. L. Sivco and A. Y. Cho: *Int. Symp. GaAs and Related Compounds, Biarritz, 1984*, Insti. Phys. Conf. Ser. No. 74, Chapter 4 (1985) p. 687.
30) J. S. Weiner, D. S. Chemla, D. A. B. Miller, T. H. Wood, D. L. Sivco and A. Y. Cho: Appl. Phys. Lett. **46** (1985) 619.
31) T. Miyazawa, S. Tarucha, Y. Ohmori, Y. Suzuki and H. Okamoto: Jpn. J. Appl. Phys. **25** (1986) L200.
32) M. Shinada and S. Sugano: J. Phys. Soc. Jpn. **21** (1966) 1936.
33) M. Matsuura and Y. Shinozuka: J. Phys. Soc. Jpn. **53** (1984) 3318.
34) Y. Masumoto, M. Matsuura, S. Tarucha and H. Okamoto: Surf. Sci. **170** (1986) 635.
35) R. C. Miller, D. A. Kleinman, W. T. Tsang and A. C. Gossard: Phys. Rev. **B24** (1981) 1134.
36) S. Tarucha, H. Okamoto, Y. Iwasa and N. Miura: Solid State Commun. **52** (1984) 815.
37) J. C. Maan, G. Belle, A. Fasolino, M. Alterelli and K. Ploog: Phys. Rev. **B30** (1984) 2253.
38) S. Tarucha H. Iwamura, T. Saku, H. Okamoto, Y. Iwasa and N. Miura: *Collected Papers of 2nd Int. Conf. (Yamada Conf.) on Modulated Semiconductor Structures, Kyoto, 1985*, p. 126, and Surf. Sci. **174** (1986) 194.
39) Y. Masumoto, S. Tarucha and H. Okamoto: J. Phys. Soc. Jpn. **55** (1986) 57.
40) D. S. Chemla, D. A. B. Miller, P. W. Smith, A. C. Gossard and W. Wiegmann: IEEE J. Quantum Electron. **QE-20** (1984) 265.
41) E. E. Mendez, G. Bastard, L. L. Chang, L. Esaki, H. Morkoç and R. Fischer: *Proc. 16th Int. Conf. Phys. Semiconductor 1982*; Physica **117–118** (1983) 711.
42) G. Bastard, E. E. Mendez, L. L. Chang and L. Esaki: Phys. Rev. **B26** (1982) 1974.
43) T. H. Wood, C. A. Burrus, Jr., D. A. B. Miller, D. S. Chemla, T. C. Damen, A. C. Gossard and W. Wiegmann: Appl. Phys. Lett. **44** (1984) 16.
44) T. H. Wood, C. A. Burrus, D. A. B. Miller, D. S. Chemla, T. C. Damen, A. C. Gossard and W. Wiegmann: IEEE J. Quantum Electron. **QE-21** (1985) 117.
45) D. A. B. Miller, D. S. Chemla, T. C. Damen, A. C. Gossard, W. Wiegmann, T. H. Wood and C. A. Burrus, Jr.: Appl. Phys. Lett. **45** (1984) 13.
46) D. A. B. Miller, D. S. Chemla, T. C. Damen, A. C. Gossard, W. Wiegmann, T. H. Wood and C. A. Burrus, Jr.: Phys. Rev. Lett. **53** (1984) 2173.
47) D. A. B. Miller, D. S. Chemla, T. C. Damen, T. H. Wood, C. A. Burrus, Jr., A. C. Gossard and W. Wiegmann: IEEE J. Quantum Electron. **QE-21** (1985) 1462.
48) D. A. B. Miller: *Collected Papers of 2nd Int. Conf. (Yamada Conference) on Modulated Semiconductor Structure, Kyoto, 1985*, p. 459, and Surf. Sci. **174** (1986) 221.
49) K. Yamanaka, T. Fukunaga, N. Tsukada, K. L. I. Kobayashi and M. Ishii: Appl. Phys. Lett. **48** (1986) 840.
50) H. Iwamura, T. Saku and H. Okamoto: Jpn. J. Appl. Phys. **24** (1985) 124.
51) K. Woodbridge, P. Blood, E. D. Fletcher and P. J. Hulyet: Appl. Phys. Lett. **45** (1984) 16.
52) D. S. Chemla, T. C. Damen, D. A. B. Miller, A. C. Gossard and W. Wiegmann: Appl. Phys. Lett. **42** (1983) 864.
53) J. P. van der Ziel, R. Dingle, R. C. Miller, W. Wiegmann and W. A. Nordland, Jr.: Appl. Phys. Lett. **26** (1975) 463.
54) R. Chin, N. Holonyak, Jr. and B. A. Vojak: Appl. Phys. Lett. **36** (1980) 19.
55) N. Holonyak, Jr., R. M. Kolbas, R. D. Dupuis and P. D. Dapkus: IEEE J. Quantum Electron. **QE-16** (1980) 170.
56) W. T. Tsang: Appl. Phys. Lett. **39** (1981) 786.
57) D. R. Scifres, C. Lindstrom, R. D. Burnham, W. Streifer and T. L. Paoli: Electron. Lett. **19** (1983) 169.
58) G. L. Harnagle, P. S. Cross, D. R. Scifres, D. P. Worland: Electron. Lett. **22** (1986) 231.
59) W. T. Tsang, C. Weisbuch, R. C. Miller and R. Dingle: Appl. Phys. Lett. **35** (1979) 673.
60) N. K. Dutta: Electron. Lett. **18** (1982) 451.
61) N. K. Dutta: J. Appl. Phys. **53** (1982) 7211.
62) N. K. Dutta, S. G. Napholtz, R. Yen, R. L. Brown, T. M. Shen, N. A. Olsson and D. C. Craft: Appl. Phys. Lett. **46** (1985) 19.
63) N. K. Dutta, S. G. Napholtz, R. Yen, T. Wessel, T. M. Shen and N. A. Olsson: Appl. Phys. Lett. **46** (1985) 1036.
64) Y. Sasai, N. Hase, M. Ogura and T. Kajiwara: *Int. Symp. GaAs and Related Compounds, Karuizawa, 1985*, Inst. Phys. Conf. Ser. No. 79. (1986) p. 709.
65) T. Yanase, Y. Kato, I. Mito, M. Yamaguchi, K. Nishi, K. Kobayashi and R. Lang: Electron. Lett. **19** (1983) 700.
66) H. Iwamura, T. Saku, H. Kobayashi and Y. Horikoshi: J. Appl.

Phys. **54** (1983) 2692.
67) M. Yamanishi and I. Suemune: Jpn. J. Appl. Phys. **23** (1984) L35.
68) M. Yamada, S. Ogita, M. Yamagishi, K. Tabata, N. Nakaya, M. Asada and Y. Suematsu: Appl. Phys. Lett. **45** (1984) 324.
69) H. Kobayashi, H. Iwamura, T. Saku and K. Otsuka: Electron. Lett. **19** (1983) 166.
70) K. Aiki, M. Nakamura and J. Umeda: IEEE J. Quantum Electron. **QE-12** (1976) 597.
71) N. K. Dutta, S. G. Napholtz, A. B. Piccirilli and G. Prgybylek: Appl. Phys. Lett. **48** (1986) 1419.
72) H. Iwamura, T. Saku, T. Ishibashi, K. Otsuka and Y. Horikoshi: Electron. Lett. **19** (1983) 180.
73) K. Uomi, N. Chinone, T. Ohtoshi and T. Kajimura: *Int. Symp. GaAs and Related Compounds, Karuizawa, Japan, 1985*, Inst. Phys. Conf. Ser. No. 79 (1986) p. 703.
74) N. K. Dutta, N. A. Olsson and W. T. Tsang: Appl. Phys. Lett. **45** (1984) 836.
75) N. K. Dutta, S. G. Napholtz, R. Yen, R. L. Brown, T. M. Shen, N. A. Olsson and D. C. Craft: Appl. Phys. Lett. **46** (1985) 19.
76) S. Tarucha, Y. Horikoshi and H. Okamoto: Jpn. J. Appl. Phys. **22** (1983) L482.
77) H. Iwamura, S. Tarucha, T. Saku, Y. Horikoshi and H. Okamoto: Jpn. J. Appl. Phys. **22** (1983) L751.
78) S. Tarucha and H. Okamoto: Appl. Phys. Lett. **48** (1986) 1.
79) S. Tarucha, Y. Horikoshi and H. Okamoto: Jpn. J. Appl. Phys. **22** (1983) L482.
80) S. Tarucha, H. Kobayashi, Y. Horikoshi and H. Okamoto: Jpn. J. Appl. Phys. **23** (1984) 874.
81) H. C. Casey, Jr. and M. B. Panish: *Heterostructure Lasers* (Academic Press, New York, 1978) Part A, p. 163.
82) N. Holonyak, Jr., W. D. Laidig and M. D. Camras: Appl. Phys. Lett. **39** (1981) 102.
83) T. Fukuzawa, S. Semura, T. Ohta, Y. Uchida, T. Narusawa, K. L. I. Kobayashi and H. Nakashima: *15th (1983) Conf. Solid State Devices and Materials, Tokyo*, C4-8LN, and Appl. Phys. Lett. **45** (1984) 1.
84) Y. Suzuki, Y. Horikoshi, M. Kobayashi and H. Okamoto: Electron. Lett. **20** (1984) 383.
85) H. Iwamura, T. Saku, Y. Hirayama and H. Okamoto: Jpn. J. Appl. Phys. **24** (1985) L101.
86) T. Saku, H. Iwamura, Y. Hirayama, Y. Suzuki and H. Okamoto: Jpn. J. Appl. Phys. **24** (1985) L73.
87) H. Iwamura, T. Saku, Y. Hirayama, Y. Suzuki and H. Okamoto: Jpn. J. Appl. Phys. **24** (1985) L911.
88) M. B. Panish and H. Temkin: Appl. Phys. Lett. **44** (1984) 785.
89) H. Temkin, K. Alavi, W. R. Wagner, T. P. Pearsall and A. Y. Cho: Appl. Phys. Lett. **42** (1983) 845.
90) H. Temkin and M. B. Panish: *Int. Symp. GaAs and Related Compounds, Karuizawa, Japan, 1985*, Inst. Phys. Conf. Ser. No. 79 (1986) p. 649.
91) Y. Ohmori, S. Tarucha, Y. Horikoshi and H. Okamoto: Jpn. J. Appl. Phys. **23** (1984) L94.
92) Y. Ohmori, Y. Suzuki and H. Okamoto: Jpn. J. Appl. Phys. **24** (1985) L657.
93) Y. Ohmori, Y. Suzuki and H. Okamoto: *Int. Symp. GaAs and Related Compounds, Karuizawa, Japan, 1985*, Inst. Phys. Conf. Ser. No. 79 (1986) p. 721.
94) Y. Suzuki, Y. Ohmori and H. Okamoto: J. Appl. Phys. **59** (1986) 3760.
95) H. M. Gibbs, S. S. Tarng, J. L. Jewell, D. A. Weinbergar, K. Tsai, A. C. Gossard, S. L. McCall and A. Passner: Appl. Phys. Lett. **41** (1982) 221.
96) T. Venkatesan, B. Wilkens, Y. H. Lee, M. Warren, G. Olbright, H. M. Gibbs, N. Peyghambarian, J. S. Smith and A. Yariv: Appl. Phys. Lett. **48** (1986) 145.
97) K. Wakita, Y. Kawamura, Y. Yoshikuni, H. Asahi and S. Uehara: Electron. Lett. **21** (1985) 951.
98) S. Tarucha, H. Iwamura, T. Saku and H. Okamoto: Jpn. J. Appl. Phys. **24** (1985) L442.
99) T. H. Wood, C. A. Burrus, R. S. Tucker, J. S. Weiner, D. A. B. Miller, D. S. Chemla, T. C. Damen, A. C. Gossard and W. Wiegmann: Electron. Lett. **21** (1985) 693.
100) Y. Silberberg, P. W. Gossard and W. Wiegmann: Opt. Lett. **9** (1984) 507.
101) P. W. Smith, Y. Silberberg and D. A. B. Miller: J. Opt. Soc. Am. **B2** (1985) 1228.
102) S. Tarucha and H. Okamoto: Appl. Phys. Lett. **49** (1986) 543.
103) W. D. Coleman, P. D. Dapkus, C. G. Kirkpatrick, M. D. Camras and N. Holonyak, Jr.: Appl. Phys. Lett. **40** (1982) 904.
104) Y. Hirayama, Y. Horikoshi and H. Okamoto: Jpn. J. Appl. Phys. **23** (1984) 1568.
105) M. Kawabe, N. Matsuura, N. Shimizu, F. Hasegawa and Y. Nannichi: *Extended Abstract of 16th (1984 Int.) Conf. Solid State Devices and Materials, Kobe, 1984* (Business Center for Academic Societies Japan, Tokyo, 1984) p. 611.
106) Y. Hirayama, Y. Suzuki and H. Okamoto: Jpn. J. Appl. Phys. **24** (1985) 1498.
107) Y. Hirayama, Y. Suzuki, S. Tarucha and H. Okamoto: Jpn. J. Appl. Phys. **24** (1985) L516.
108) Y. Hirayama, Y. Suzuki and H. Okamoto: *Collected Papers of 2nd Int. Conf. (Yamada Conf.) on Modulated Semiconductor Structure, Kyoto, 1985*, p. 266, and Surf. Sci. **174** (1986) 98.
109) R. L. Seliger, J. W. Ward, V. Wang and R. K. Kubena: Appl. Phys. Lett. **34** (1979) 310.
110) T. Shiokawa, P. H. Kim, K. Toyoda, S. Namba, T. Matsui and K. Gamo: J. Vac. Sci. & Technol. **B1** (1983) 1117.
111) H. Hashimoto and E. Miyauchi: *Extended Abstract of 16th (1984 Int.) Conf. Solid State Devices and Materials, Kobe, 1984* (Business Center for Academic Societies Japan, Tokyo, 1984) p. 121.
112) Y. Hirayama and H. Okamoto: Jpn. J. Appl. Phys. **24** (1985) L965.
113) K. Nakamura, T. Nozaki, T. Shiokawa, K. Toyoda and S. Namba: Jpn. J. Appl. Phys. **24** (1985) L903.
114) Y. Arakawa, K. Vahala and A. Yariv: *Extended Abstract of 2nd Int. Conf. (Yamada Conf.) on Modulated Semiconductor Structure, Kyoto, 1985*, p. 88, and Surf. Sci. **174** (1986) 155.
115) M. Asada, Y. Miyamoto and Y. Suematsu: Jpn. J. Appl. Phys. **24** (1985) L95.
116) T. Kodama, Y. Osaka and M. Yamanishi: Jpn. J. Appl. Phys. **24** (1985) 1370.
117) M. Matsuura and T. Kamizato: *Extended Abstract of 2nd Int. Conf. (Yamada Conf.) on Modulated Semiconductor Structure, Kyoto, 1985*, p. 102, and Surf. Sci. **174** (1986) 183.
118) P. M. Petroff, A. C. Gossard, R. A. Logan and W. Wiegmann: Appl. Phys. Lett. **41** (1982) 635.
119) K. Kash, A. Scherer, J. M. Worlock, H. G. Craighead and M. C. Tamargo: Appl. Phys. Lett. **49** (1986) 1043.
120) J. Cibert, P. M. Petroff, G. J. Dolan, S. J. Pearton, A. C. Gossard and J. H. English: Appl. Phys. Lett. **49** (1986) 1275.